Corrosion Science 50 (2008) 3629–3647

Contents lists available at ScienceDirect

Corrosion Science

journal homepage: www.elsevier.com/locate/corsci

A general model for the repassivation potential as a function of multiple aqueous species. 2. Effect of oxyanions on localized corrosion of Fe–Ni–Cr–Mo–W–N alloys

A. Anderko [a,*], N. Sridhar [b], M.A. Jakab [c], G. Tormoen [c]

[a] OLI Systems, 108 American Road, Morris Plains, NJ 07950, USA
[b] Det Norske Veritas, 5777 Frantz Road, Dublin, OH 43017, USA
[c] Southwest Research Institute, 6220 Culebra Road, San Antonio, TX 78238, USA

ARTICLE INFO

Article history:
Received 26 August 2008
Accepted 29 August 2008
Available online 6 September 2008

Keywords:
A. Stainless steels
A. Nickel-base alloys
B. Modeling studies
C. Crevice corrosion
C. Pitting corrosion

ABSTRACT

A recently developed model for predicting the repassivation potential has been applied to stainless steels and nickel-base alloys in aqueous environments containing chlorides and various inhibiting anions. The model accounts for the effects of solution chemistry and temperature on the repassivation of localized corrosion by considering competitive dissolution, adsorption, and oxide formation processes at the interface between the metal and the occluded site solution. An extensive database of repassivation potentials has been established for six alloys (UNS 31603, N06600, N06690, S31254, S32205, and UNS S41425) in contact with solutions that combine chlorides with hydroxides, molybdates, vanadates, sulfates, nitrates, and nitrites at various concentrations and temperatures. Also, repassivation potentials are reported for four alloys (UNS N08367, N08800, N06625, and N10276) in chloride solutions. The database has been used to establish the parameters of the model and verify its accuracy. The model quantitatively predicts the transition between concentrations at which localized corrosion is possible and those at which inhibition is expected. It is capable of predicting the repassivation potential over wide ranges of experimental conditions using parameters that can be generated from a limited number of experimental data. The parameters of the model have been generalized as a function of alloy composition, thus making it possible to predict the repassivation potential for alloys that have not been experimentally investigated.

1. Introduction

Predictive modeling of localized corrosion is very challenging because of the large number of factors that influence the nucleation, growth and repassivation of pits or crevice corrosion sites. Among the key factors, properties of chemical species in an aqueous environment, concentrations of components, alloy composition, and temperature are of particular importance. In the last four decades, considerable progress was made in understanding the mechanisms of localized corrosion of various metallic materials [1–6]. At the same time, various modeling methodologies have been developed by considering atomic or molecular processes, microstructural features, and transport processes in macroscopic cavities.

In our previous papers [7,8], a comprehensive computational model has been proposed to predict the tendency of metals to undergo localized corrosion as a function of environmental conditions. To predict the occurrence of localized corrosion, this approach relies on calculating two characteristic parameters as functions of solution chemistry, i.e., (1) the corrosion potential and (2) the repassivation potential, also called the protection potential. The repassivation potential (E_{rp}, or E_{rcrev}, depending on whether one measures the potential of a boldly exposed or creviced specimen) is a measure of the tendency of an alloy to undergo localized corrosion in a given environment. In this paper, the two repassivation potentials are referred to by the common notation of E_{rp}, because they coincide at high pit depths [9]. It has been shown in previous papers [7,9,10] that E_{rp} is the potential below which stable pitting or crevice corrosion does not occur. Also, E_{rp} is relatively insensitive to surface finish as well as prior pit depth as long as propagation exceeds a certain minimum value. The predicted repassivation potential is then compared to the corrosion potential (E_{corr}) in the same environment to determine the susceptibility of an alloy to localized corrosion [7,9]. The separation of modeling into these two steps is valid as long as the initiation of stable localized corrosion is considered because the corrosion potential is not affected at this stage by the localized corrosion processes and the interaction between pits can be ignored. Such a separation remains valid as long as significant pit or crevice corrosion growth does not occur and the area of actively corroding pits does not become significant compared to the overall area.

* Corresponding author. Tel.: +1 973 539 4996x25; fax: +1 973 539 5922.
E-mail address: aanderko@olisystems.com (A. Anderko).

0010-938X/$ - see front matter © 2008 Elsevier Ltd. All rights reserved.
doi:10.1016/j.corsci.2008.08.046

The key to the practical application of this predictive approach is the accurate computation of the repassivation potential as a function of environmental conditions. For this purpose, a mechanistic model was developed in a previous paper [7]. This model was demonstrated to yield accurate results for a number of alloys in well-defined laboratory solutions [7] and in complex chemical process environments [11]. Also, it was shown to provide an estimate of the maximum propagation rate of individual pits. An important feature of this model is its capability of relating the key parameters that determine localized corrosion to the chemistry of aqueous environments. In this context, the environmental species can be classified as aggressive, non-aggressive, or inhibitive depending on their effect on the repassivation potential. Aggressive species, such as chloride, lower the repassivation potential whereas inhibitive species, such as nitrate, may significantly increase it. Non-aggressive species, such as acetate, may be considered as "diluent" species in that they only slightly affect the repassivation potential. Such a classification is only for reference purposes because the degree of influence of a chemical species may depend on other parameters, such as temperature and alloy composition.

In this study, we continue the development of the repassivation potential model by focusing on systems containing various inorganic oxyanions in addition to chlorides. Several studies have shown that various inorganic anions such as nitrate, sulfate or carbonate can inhibit localized corrosion of Fe–Ni–Cr–Mo alloys [2,12–18]. In general, the effectiveness of the inhibition is a complex function of the concentrations of both aggressive and inhibitive ions, temperature, and the chemical nature of the anions. In a previous paper [7], it has been shown that the repassivation potential shows an abrupt transition as a function of inhibitor concentration. This transition, which can be reproduced by the E_{rp} model, can be identified with the threshold condition for inhibition. Thus, it is of great interest to investigate the interplay of aggressive and inhibitive species in a systematic way to develop a methodology for predicting the conditions at which localized corrosion is possible and those at which it cannot occur. The objective of this study is to develop such a methodology for Fe–Cr–Ni–Mo–W–N alloys in the presence of common inhibiting oxyanions, i.e., hydroxides, molybdates, vanadates, sulfates, nitrates, and nitrites.

For this purpose, we first develop an experimental database of repassivation potentials of several stainless steels and nickel-base alloys (316L, 600, 690, 254SMO, 2205, and s-13Cr) at selected temperatures for various chloride/inhibitor combinations. Also, we report E_{rp} data for an additional four alloys (AL6XN, 800, 625, and 276) in chloride-only solutions. Then, the database is used to calibrate and verify the repassivation potential model. Further, the model is established as a tool for determining the compositions for which the inhibitors can be expected to be effective. Finally, in order to enhance the predictive character of the model, we develop a generalized correlation for calculating the repassivation potential as a function of alloy composition in chloride and chloride–oxyanion environments.

2. Experimental

2.1. Measurement of the repassivation potential

The experimental procedures for measuring repassivation potentials were described previously [7–9]. Tests were conducted in glass kettles fitted with a PTFE lid containing a number of ports for the specimen, reference electrodes, counter electrode, thermocouple, and gas bubbler. Nitrogen gas was purged throughout the test. A saturated calomel electrode kept at room temperature and connected to the test solution through a Luggin probe was used as the reference electrode. The crevice corrosion repassivation potential was obtained using specimens fitted with serrated crevice washers made of polytetrafloroethylene (PTFE). Crevices were created on 3 mm thick sheet samples by clamping serrated PTFE washers (12 teeth per side) using alloy C-276 (UNS N10276) bolts isolated through PTFE sleeves at an initial torque of 0.14 N m. Only the crevice portion of the specimen was immersed in the solution, taking care not to expose the area where electrical connection to the specimen was made. Two different test procedures were followed:

1. Potential staircase method: the samples were held potentiostatically at potentials ranging from $0.642V_{SHE}$ to $0.842V_{SHE}$, such that the current density increased with time at this potential, which was indicative of localized corrosion growth. After a fixed charge density of 20.6 C/cm^2 was passed or if the time exceeded 24 h at this potential, the potential was lowered at a slow scan rate of 0.167 mV/s. The repassivation potentials were defined as potentials at which the current density was equal to 10^{-2} A/m^2. If no localized corrosion occurred at $0.642V_{SHE}$, this potential was recorded as "the repassivation potential", although this term is not valid in such cases.
2. The cyclic potentiodynamic polarization (CPP) method: the ASTM G-61 procedure was followed by scanning the potential at a scan rate of 0.167 mV/s from the open-circuit potential until a current density of 0.5 mA/cm^2 was attained. The scan was then reversed and the potential at which the current density was 10^{-2} A/m^2 was used as the repassivation potential. The charge density passed in this test varied depending on the pit initiation potential and ranged from 0.5 C/cm^2 to 1.5 C/cm^2.

Each of these methods has advantages and disadvantages. The potential staircase method has been shown to yield a truer value of the repassivation potential for the more corrosion resistant alloys (e.g. UNS N10276) [8]. This is because it was observed that when the potential was held at values higher than $1.042V_{SHE}$, localized corrosion did not occur, but instead transpassive dissolution resulted. The CPP scan for these alloys often resulted in the application of potential in the transpassive regime, because sufficient time was not given at lower potentials for localized corrosion to initiate. Furthermore, the charge density passed in a CPP test may not be sufficient to obtain a repassivation potential independent of pit depth. Unfortunately, the potentiostatic hold point of $0.642V_{SHE}$ to initiate localized corrosion in the potential staircase method is not suitable for all alloy–environment combinations. If localized corrosion does not initiate within the 24 h time period, no repassivation potential is measured in this test. The CPP method does not require the pre-determination of the potential for growing localized corrosion as the potential is scanned continuously. For the lower corrosion resistant alloys (e.g., UNS S31603), these two methods seem to yield values within the scatter band for these measurements.

Following the tests, the samples were examined visually for signs of crevice corrosion and the number of crevice corrosion sites was recorded. The total area of the specimen was used for calculating the nominal current density.

2.2. Scope of measurements

The repassivation potentials have been obtained for 316L stainless steel (UNS 31603), alloy 600 (UNS N06600), alloy 690 (UNS N06690), alloy 254SMO (UNS S31254), 2205 duplex stainless steel (UNS S32205), and Super 13Cr (S-13Cr) stainless steel (UNS S41425) in mixed aqueous solutions containing chloride ions and the following oxyanions: hydroxides, molybdates, sulfates, vana-

dates, nitrates, and nitrites. All ions were introduced as sodium salts. The repassivation potentials are also reported for alloys AL6XN (UNS N08367), 800 (UNS N08800), 625 (UNS N06625), and 276 (UNS N10276) in chloride-only solutions. The compositions of the alloys are given in Table 1. In addition to the repassivation potential data obtained in this study, literature data for alloys 22 (UNS N06022), 825 (UNS 08825) and type 304L stainless steel (UNS S30403) were also used in modeling and, therefore, these alloys are included in Table 1 for completeness.

The test conditions are summarized in Table 2. In case of the alloys for which oxyanion effects were investigated (i.e., 316L, 600, 690, 254SMO, 2205, and S-13Cr), the E_{rp} values are reported first for chloride-only environments, followed by those for mixed solutions containing oxyanions. Most of the data for alloys in mixed chloride–oxyanion environments have been obtained at 296 K and 333 K, with selected additional data measured at 323 K and 368 K. This range of temperatures made it possible to evaluate the temperature dependence of the inhibitor effects while avoiding the complications due to experimentation in pressurized vessels at temperatures above 373 K.

For each alloy–oxyanion combination, E_{rp} data were measured at several concentrations ranging from 0.0001 M to 4 M, with the majority of measurements taken at 0.004, 0.04, 0.42, and 4 M Cl^-. The actual chloride ion concentrations were selected in accordance with the resistance of a particular alloy to localized corrosion. For each chloride ion concentration, the oxyanion concentrations were selected to bracket the concentration at which localized corrosion becomes inhibited by the oxyanion. To keep the scope of the experimental study within manageable limits, the matrix of six alloys and six oxyanions was not investigated in its entirety. The effect of five oxyanions (i.e., OH^-, MoO_4^{2-}, SO_4^{2-}, VO_3^-, and NO_3^-) was studied for alloys 316L and 690. The chloride concentration–oxyanion concentration – temperature space was sampled in particular detail for type 316L stainless steel. Thus, the results for 316L SS serve as a prototype data set to which the remaining data sets could be compared. Additionally, repassivation potentials of 316L SS have been measured in nitrite solutions to compare the effect of nitrites with that of nitrates. For alloy 600, E_{rp} data were obtained for mixtures with the OH^-, MoO_4^{2-}, SO_4^{2-}, and VO_3^- ions. For alloy 254SMO, the effects of the OH^-, MoO_4^{2-}, SO_4^{2-}, and NO_3^- ions were investigated. A more limited data set was obtained for alloy 2205, for which the OH^-, MoO_4^{2-}, SO_4^{2-} ions were studied. For the S-13Cr stainless steel, only the effect of the NO_3^- ions was investigated. Together with literature data for alloy 22 [16,17], this experimental matrix makes it possible to elucidate the overall trends in the behavior of alloys in chloride–oxyanion systems and to establish a generalized correlation between the repassivation potential and alloy composition.

Experimentally determined E_{rcrev} values are reported here as single-value data. The reproducibility of E_{rcrev} data depends on the ion concentration, or more generally, the aggressiveness of the solution and test parameters, such as the crevice tightness and total charge passed. For CPP tests, the E_{rcrev} value has been shown to have an error of about ±40 mV [8,34]. For potential staircase tests, the dispersion has been somewhat less, ranging from ±10 mV to ±20 mV, depending on the anion concentration, and the values reported herein should be assumed to hold similar precision.

3. Computational model

3.1. Fundamentals of the model

In a previous paper [7], a mechanistic model was developed for calculating the repassivation potential as a function of solution chemistry and temperature. The model was derived by considering the dissolution of a metal in a localized corrosion environment in the limit of repassivation. According to the model, the metal (M) undergoes dissolution underneath a layer of concentrated metal halide solution MX. The concentrated solution may or may not be saturated with respect to a hydrous solid metal halide salt film. In the process of repassivation, a thin layer of oxide is assumed to form at the interface between the metal and the hydrous metal halide. The model assumes that, at a given instant, the oxide layer covers a certain fraction of the metal surface. This fraction increases as repassivation is approached. The dissolution rate of the metal under the oxide is lower than at the metal-halide interface and corresponds to the passive dissolution rate. Thus, as the repassivation potential is approached, the dissolution rate tends towards the passive dissolution rate. Further, the model includes the effects of multiple aggressive and non-aggressive or inhibitive species, which are taken into account through a competitive adsorption scheme. The aggressive species form metal complexes, which dissolve in the active state. On the other hand, the inhibitive species and water contribute to the formation of oxides, which induce passivity. In general, the equations that describe these processes are complex and can only be solved numerically. However, a closed-form equation has been found in the limit of repassivation, i.e., when the current density reaches a predetermined low value i_{rp} (assumed to be $i_{rp} = 10^{-2}$ A/m^2) and the fluxes of metal ions become small and comparable to those for passive dissolution. Since the objective of this paper is to apply this model to calculating E_{rp} of Fe–Ni–Cr–Mo–

Table 1
Compositions of the alloys studied (wt%)

Alloy	UNS No	Ni	Fe	Cr	Mo	W	N	C	Other
316L	S31603	10.26	Bal.	16.79	2.09	0	0.041	0.021	Cu 0.35, Mn 1.34, P 0.03, S 0.002, Si 0.47
2205	S32205	5.80	Bal.	22.50	3.20	0	0.164	0.017	Mn 1.55, P 0.02, S 0.001, Si 0.41
s-13Cr	S41425	5.90	Bal.	12.10	1.90	0	0	0.010	
254SMO[a]	S31254	18.00	Bal.	20.00	6.25	0	0.20	0.020	Cu 0.75, Mn < 1.0, Si < 1.0
AL6XN	N08367	23.88	Bal.	20.47	6.26	0	0.23	0.020	Cu 0.20, Mn 0.3, P 0.021, S 0.0003, Si 0.33
600	N06600	Bal.	9.69	15.66	0	0	0	0.020	Al < 0.17, Co < 0.06, Cu 0.20, Mn 0.28, Nb 0.02, P < 0.009, S < 0.001, Si < 0.04, Ta < 0.01, Ti < 0.31
690	N06690	Bal.	10.13	29.60	0	0	0	0.029	Al 0.21, Cu < 0.01, Mn 0.15, P 0.003, S 0.001, Si 0.02, Ti 0.34
800	N08800	32.21	Bal.	19.48	0	0	0	0.07	Al 0.48, Cu 0.23, Mn 0.95, S < 0.001, Si 0.27, Ti 0.53
825	N08825	Bal.	29.91	22.72	3.33	0	0	<0.01	Al 0.10, Cu 1.70, Mn 0.34, S < 0.001, Si 0.32, Ti 0.95
625	N06625	Bal.	2.93	21.97	8.9	0	0	0.01	Al 0.25, Mn 0.05, Nb 3.52, P 0.005, S < 0.001, Si 0.04, Ti 0.24, Ta 0.01
C-276	N10276	Bal.	6.00	15.90	16.05	3.29	0	0.002	Co 0.56, Cu 0.09, Mn 0.26, P 0.003, S 0.002, Si 0.03, V 0.16
C-22[b]	N06022	Bal.	3.82	21.24	13.43	2.85	0	0.003	Co 0.48, Mn 0.3, P 0.006, S 0.001, V 0.17, Si 0.035
304	S30403	9.05	Bal.	18.18	0.16	0	0	0.043	Cu 0.15, Mn 1.02, P 0.032, S 0.002, Si 0.65

[a] Registered Trademark of Avesta Polarit.
[b] Registered Trademark of Haynes International.

Table 2
Crevice repassivation potentials measured for alloys 316L, 600, 690, 254SMO, 2205, and s-13Cr in aqueous chloride–oxyanion solutions and alloys 625, 276, AL6XN, and 800 in chloride solutions

Alloy	Oxyanion	Temperature (K)	M (Cl^-) mol/L	M (oxyanion) mol/L	E_{rp}mV (SCE)
316L	None	296.15	0.004		No localized corrosion
			0.42		−67
			0.42		−137
			3		−200
			4		−408
			4		−305
		333.15	0.0001		220
			0.001		−90
			0.04		−115
			0.04		−87
			0.42		−225
			0.5		−214
		368.15	0.5		−270
	OH^-	296.15	0.004	0.004	No localized corrosion
				0.04	No localized corrosion
				0.4	No localized corrosion
			0.5	0.1	−168
				0.25	No localized corrosion
				0.5	−101
				0.75	No localized corrosion
				1	No localized corrosion
			4	0.0625	−221
				0.5	−300
				1	−408
				1.75	−349
		333.15	0.04	0.004	−321
			0.04	0.04	−139
			0.04	0.04	−25
			0.04	0.4	No localized corrosion
			0.04	0.4	−19
			0.42	0.04	−240
			0.42	0.4	390
	MoO_4^{2-}	296.15	0.004	0.04	No localized corrosion
				0.1	No localized corrosion
				0.4	No localized corrosion
			0.42	0.04	−119
				0.4	−94
				0.4	No localized corrosion
				1.5	No localized corrosion
			4	0.4	−210
				1.5	−228
		333.15	0.04	0.0004	−120
				0.004	−78
				0.04	No localized corrosion
				0.1	No localized corrosion
				0.4	No localized corrosion
			0.42	0.04	−42
				0.4	−137
				1.5	−177
	SO_4^{2-}	296.15	0.004	0.04	No localized corrosion
				0.4	No localized corrosion
			0.1	0.42	No localized corrosion
			0.42	0.04	−58
				0.21	−105
				0.4	−167
				0.42	−48
				1	−83
		333.15	0.04	0.004	−151
				0.04	23
				0.1	−91
				0.4	−57
				0.4	No localized corrosion
				1	No localized corrosion
	VO_3^-	296.15	0.004	0.04	No localized corrosion
				0.4	No localized corrosion
			0.42	0.04	−129
				0.04	−152
				0.2	−113
				0.2	No localized corrosion
				0.4	14
				0.4	−116
				1.4	No localized corrosion

Table 2 (*continued*)

Alloy	Oxyanion	Temperature (K)	M (Cl^-) mol/L	M (oxyanion) mol/L	E_{rp}mV (SCE)
		333.15	0.04	0.004	−70
				0.04	−51
				0.4	No localized corrosion
	NO_3^-	296.15	0.42	0.021	−107
				0.042	−110
				0.063	−81
				0.073	−81
				0.084	−63
				0.105	−32
				0.168	No localized corrosion
				0.21	−56
				0.21	No localized corrosion
				0.252	No localized corrosion
				0.42	No localized corrosion
			3	0.5	−160
				1.5	−143
				3	−131
				4	No localized corrosion
				5	No localized corrosion
			4	2.4	−212
				3	−204
			0.04	0.4	No localized corrosion
		368.15	0.42	0.252	−88
				0.315	−70
				0.42	−52
				0.63	61
				0.84	No localized corrosion
			4	2.4	−256
	NO_2^-	296.16	0.42	0.004	−0.123
				0.01	0.042
				0.04	No localized corrosion
				0.4	No localized corrosion
			4	0.4	−0.164
				2	0.015
		333.15	0.04	0.4	No localized corrosion
600	None	296.15	4		−319
		333.15	0.0001		67
			0.001		−4
			0.01		−80
			0.04		−82
			0.04		−281
			0.04		−80
			0.5		−222
		368.15	0.5		−436
	OH^-	296.15	4	0.4	−155
				0.4	−254
				0.4	−101
				0.4	−166
				2	−194
				2	−166
				2	−194
		333.15	0.04	0.04	−170
				0.04	−207
				0.04	−175
				0.4	−96
	MoO_4^{2-}	296.15	4	0.4	−153
				1.5	−169
				1.5	−170
		333.15	0.04	0.004	−51
				0.01	−97
				0.01	−71
				0.04	−86
				0.04	No localized corrosion
				0.2	No localized corrosion
				0.32	No localized corrosion
				0.4	No localized corrosion
	SO_4^{2-}	296.15	4	0.4	−251
				2	−289
				2	−284
		333.15	0.04	0.004	−112
				0.004	−114
				0.04	−77
				0.04	−83
				0.04	−112

(*continued on next page*)

Table 2 (*continued*)

Alloy	Oxyanion	Temperature (K)	M (Cl^-) mol/L	M (oxyanion) mol/L	E_{rp}mV (SCE)
				0.1	−48
				0.1	−45
				0.2	No localized corrosion
				0.32	No localized corrosion
				0.4	No localized corrosion
	VO_3^-	333.15	0.04	0.04	−40
690	None	296.15	4		−169
			4		−178
	None	333.15	0.0001		456
			0.001		64
			0.01		86
			0.04		−219
			0.04		−224
			0.04		−112
			0.1		−77
			1		−288
			4		−291
			4		−292
	OH^-	296.15	4	0.4	−189
				1	−387
				1	−234
				1.5	−236
		333.15	0.04	0.04	−146
				2	−153
			4	0.4	−376
				2	−363
				2	−365
	MoO_4^{2-}	296.15	4	0.4	−165
				1.5	−113
		333.15	0.04	0.004	−212
				0.004	−215
				0.01	−87
				0.04	43
				0.4	No localized corrosion
			4	0.4	−300
				1.5	−324
	VO_3^-	333.15	0.04	0.04	−84
				0.04	−275
				0.2	No localized corrosion
				0.32	No localized corrosion
				0.4	No localized corrosion
	SO_4^{2-}	296.15	4	0.4	−278
				1.5	−207
		333.15	0.04	0.04	−51
				0.04	−275
				0.2	No localized corrosion
				0.32	No localized corrosion
				0.4	No localized corrosion
	NO_3^-	333.15	0.1	0.05	−59
				0.1	33
				0.5	No localized corrosion
254SMO	None	323.15	0.001		384
			0.005		50
			0.01		48
			0.1		5
			0.1		−4
		333.15	0.001		362
			0.01		45
			0.4		−28
			0.5		−33
			4		−228
		368.15	0.5		−6
					−165
	OH^-	333.15	4	0.4	No localized corrosion
				2	−261
	MoO_4^{2-}	333.15	0.4	0.004	−83
				0.01	−81
				0.04	38
				0.1	−67
				0.1	No localized corrosion
				0.5	No localized corrosion
				1	No localized corrosion
			4	0.4	−106
				1.5	−193

Table 2 (*continued*)

Alloy	Oxyanion	Temperature (K)	M (Cl^-) mol/L	M (oxyanion) mol/L	E_{rp}mV (SCE)
	SO_4^{2-}	296.15	0.677	0.0354	No localized corrosion
		323.15	0.169	0.0354	−22
				0.0354	−109
				0.0354	−75
			0.677	0.0083	−129
				0.0083	−179
		333.15	4	0.4	−238
				2	−190
	NO_3^-	333.15	0.1	0.1	324
			0.5	0.5	345
2205	None	333.15	0.04		390
			0.4		−185
			4		−331
	OH^-	333.15	0.04	0.04	No localized corrosion
				0.4	No localized corrosion
				1	No localized corrosion
			4	1	0
	MoO_4^{2-}	333.15	0.4	30.004	−119
				0.01	−100
				0.04	No localized corrosion
			4	0.4	−216
				1.5	−251
				1.5	−267
	SO_4^{2-}	333.15	0.04	0.04	No localized corrosion
			0.4	0.004	−197
				0.01	−51
			4	0.4	−282
				0.4	−294
				2	−302
s-13Cr	None	296.15	0.0001		−33
			0.0001		181
			0.001		−214
			0.001		−22
			0.01		−185
			0.1		−292
		333.15	0.0001		−65
			0.001		−197
			0.5		−377
		368.15	0.5		−337
	NO_3^-	296.15	0.001	0.001	−56
			0.01	0.01	49
				0.1	No localized corrosion
			0.1	0.1	−116
				1	No localized corrosion
276	None	333.15	0.1		283
			0.5		128
			4		15
			6		−55
		368.15	0.1		205
			0.5		121
			1		109
			4		−181
			6		−262
625	None	333.15	0.5		206
			0.5		460
			9		−264
			11.5		−318
		368.15	0.028		299
			0.028		No localized corrosion
			0.1		−123
			0.1		199
			0.3		−205
			0.5		47
			1		−60
			1		−216
			1		−142
			1		−232
			1		−219
			4		−253
			4		−177
			4		−214
			4		−259
			9		−272

(*continued on next page*)

Table 2 (*continued*)

Alloy	Oxyanion	Temperature (K)	M (Cl^-) mol/L	M (oxyanion) mol/L	E_{rp}mV (SCE)
				11.5	−310
AL6XN	None	333.15	0.001		No localized corrosion
			0.005		227
			0.01		112
			0.1		122
			0.5		−9
			1		−20
			4		−229
			6		−261
		368.15	0.001		No localized corrosion
			0.005		107
			0.01		89
			0.1		−85
			0.5		−179
			1		−211
			4		−267
			6		−290
800	None	333.15	0.0001		No localized corrosion
			0.001		167
			0.01		12
			0.1		−201
			0.5		−177
			1		−199

W–N alloys in various aqueous chloride-oxyanion systems, we summarize here the parameters that need to be determined to apply the model in practice. These parameters will be evaluated on the basis of the experimentally obtained matrix of E_{rp} data. Further, they will be generalized in terms of alloy composition.

The repassivation potential model yields a closed-form expression, which can be solved numerically to calculate E_{rp} if the model parameters are known. For a system containing NA aggressive ions and NI inhibitive ions, this equation is given in its most general form by

$$1+\sum_{k}^{\mathrm{NI}}\left[\left(\frac{i_{rp}}{i_p}-1\right)\frac{l''_k}{i_{rp}}\right]\theta_k^{n_k}\exp\left(\frac{\xi_k \mathrm{FE_{rp}}}{\mathrm{RT}}\right)=\sum_{j}^{\mathrm{NA}}\frac{k''_j}{i_{rp}}\theta_j^{n_j}\exp\left(\frac{\alpha_j \mathrm{FE_{rp}}}{\mathrm{RT}}\right) \quad (1)$$

where i_p is the passive current density, i_{rp} is the experimental current density that defines repassivation ($i_{rp} = 10^{-2}$ A/m^2), θ_j is the partial surface coverage fraction by solution species j, T is the temperature, R is the gas constant, F is the Faraday constant and $k''_j, l''_k, n_j, n_k, \alpha_j$, and ξ_k are electrochemical kinetic parameters as defined below. The summation on the right-hand side of Eq. (1) is performed over all aggressive species ($j = 1 \ldots$, NA) and the summation on the left-hand side pertains to inhibitive species ($k = 1 \ldots$, NI). It should be noted that H_2O molecules are treated as inhibitive species because they contribute to the formation of the oxide layer. The electrochemical parameters of the model are defined as follows:

(i) The quantity k''_j is the reaction rate constant for alloy dissolution mediated by the adsorption of aggressive species j. This constant is used in a scaled form (i.e., as $k_j = k''_j/i_{rp}$) and is expressed using a scaled Gibbs energy of activation $\Delta g^{\neq}_{A,j}$:

$$k_j=\frac{k''_j}{i_{rp}}=\exp\left(-\frac{\Delta g^{\neq}_{A,j}}{\mathrm{RT}}\right) \quad (2)$$

The quantity $\Delta g^{\neq}_{A,j}$ is introduced in order to express the temperature dependence of the rate constant in a convenient thermodynamic form.

(ii) The quantity l''_k is the reaction rate constant for the formation of oxide mediated by the adsorption of inhibitive species k. As with the k''_j constant, it is used in a scaled form (i.e., as $l_k=\left(\frac{i_{rp}}{i_p}-1\right)\frac{l''_k}{i_{rp}}$) and is expressed using a scaled Gibbs energy of activation $\Delta g^{\neq}_{I,k}$

$$l_k=\left(\frac{i_{rp}}{i_p}-1\right)\frac{l''_k}{i_{rp}}=\exp\left(-\frac{\Delta g^{\neq}_{I,k}}{\mathrm{RT}}\right) \quad (3)$$

(iii) The quantities n_j and n_k. are the reaction rate orders with respect to the aggressive species j and inhibitive species k, respectively. It has been found in previous studies that n_k can be assigned a default value of one in practical applications of the model.

(iv) The parameters α_j and ξ_k are the electrochemical transfer coefficients for the reactions involving the aggressive species j and inhibitive species k, respectively. The parameter α_j can be assumed to be equal to one for simplicity.

The partial coverage fraction of a species j is related to the activity of this species in the bulk solution through an adsorption isotherm, i.e.,

$$\theta_j=\frac{r_j a_j}{1+\sum_k r_k a_k} \quad (4)$$

where the adsorption coefficient is defined using the Gibbs energy of adsorption $\Delta G_{ads,i}$, i.e.,

$$r_j=\exp\left(-\frac{\Delta G_{ads,j}}{\mathrm{RT}}\right) \quad (5)$$

The latter property can be assigned a common default value for the majority of species although specific parameters may be needed for strongly adsorbing species. For H_2O in aqueous solutions, θ_{H_2O} is assumed to be equal to one for simplicity.

For calculating the temperature dependence of the kinetic parameters, the scaled Gibbs energies of activation may be further related to temperature as

$$\frac{\Delta g^{\neq}_{A,j}}{T}=\frac{\Delta g^{\neq}_{A,j}(T_{ref})}{T_{ref}}+\Delta h^{\neq}_{A,j}\left(\frac{1}{T}-\frac{1}{T_{ref}}\right) \quad (6)$$

for aggressive ions and

$$\frac{\Delta g^{\neq}_{I,k}}{T}=\frac{\Delta g^{\neq}_{I,k}(T_{ref})}{T_{ref}}+\Delta h^{\neq}_{I,k}\left(\frac{1}{T}-\frac{1}{T_{ref}}\right) \quad (7)$$

for water and inhibitive species. In Eqs. (6) and (7), the parameters $\Delta g^{\neq}_{A,j}(T_{\mathrm{ref}})$ and $\Delta g^{\neq}_{I,k}(T_{\mathrm{ref}})$ are the scaled Gibbs energies of activation at reference temperature T_{ref} = 298.15 K for the reactions mediated by the adsorption of aggressive and inhibitive ions, respectively. The quantities $\Delta h^{\neq}_{A,j}$ and $\Delta h^{\neq}_{I,k}$ are the corresponding enthalpies of activation.

3.2. Determination of model parameters

In a practical implementation of the model, the parameters are determined as follows:

(1) Since E_{rp} data are most abundant for chloride solutions, the scaled Gibbs energy of activation for chloride ions ($\Delta g^{\neq}_{A,\mathrm{Cl}}$), the reaction order with respect to chlorides (n_{Cl}), the scaled Gibbs energy of activation for water ($\Delta g^{\neq}_{I,\mathrm{H_2O}}$), and the electrochemical transfer coefficient for water ($\xi_{\mathrm{H_2O}}$) are determined based on data for chloride-only solutions, using Eqs. (1) and (2). It will be later shown in this study that this procedure can be simplified by the fact that the n_{Cl} and $\xi_{\mathrm{H_2O}}$ parameters can be assigned nearly-universal values for Fe–Ni–Cr–Mo–W–N alloys and do not necessarily need to be individually determined. If the temperature range of the data is sufficient to establish the temperature dependence of the Gibbs energies of activation, the enthalpies of activation $\Delta h^{\neq}_{A,\mathrm{Cl}}$ and $\Delta h^{\neq}_{I,\mathrm{H2O}}$ may also be determined according to Eqs. (6) and (7). Otherwise, they are estimated using the $\Delta h^{\neq}_{A,\mathrm{Cl}}$ and $\Delta h^{\neq}_{I,\mathrm{H_2O}}$ values for a similar alloy.

(2) If the system contains aggressive species other than chlorides (e.g., bromides), the $\Delta g^{\neq}_{A,j}$ and, if necessary, n_j parameters are determined for such species using E_{rp} data for either pure or mixed solutions containing such ions. Such cases were examined in a previous study [7] and will not be considered here.

(3) The $\Delta g^{\neq}_{I,k}$ and ξ_k parameters for inhibitive ions k are determined on the basis of data for mixed solutions containing chlorides and inhibitors. Data for mixed systems are necessary because E_{rp} is undefined in solutions containing only inhibitors. The parameter ξ_k can be assigned a common default value for all the inhibiting ions studied here. If necessary, the activation enthalpy $\Delta h^{\neq}_{I,k}$ is also determined to reproduce the temperature dependence of the inhibition effect.

Table 3 summarizes the model parameters and their physical meaning. In Section 4.1, we apply the model to individual alloys in chloride–oxyanion solutions and determine the values of the parameters on the basis of the best fit to experimental data. Further, in Section 4.2, we generalize the parameters in terms of alloy composition.

4. Results and parameter development

4.1. Repassivation potential data

Table 2 contains the measured repassivation potential values for all alloy–chloride–oxyanion combinations that have been investigated. For certain conditions, the measurements have been repeated. The repeats were performed primarily in regions where there are strong gradients of the repassivation potential as a function of either oxyanion or chloride concentrations. Such strong gradients imply increased uncertainty of E_{rp}, which may be affected by small variations in solution composition. In some cases, the replicated measurements revealed substantial variability at conditions at which localized corrosion may or may not occur depending on small variations of either the oxyanion or chloride concentration. In such cases, the data were analyzed and model parameters were determined in a conservative way, i.e., by giving higher weights to the lower E_{rp} values. This ensures that the resulting model yields conservative predictions of the repassivation potential. All replicated measurements are given explicitly in Table 2. If no repeats are listed, a single measurement was performed at a given condition.

4.2. Application of the model to individual ions in chloride – oxyanion environments

To analyze the effect of chlorides and oxyanions on the repassivation potential, we first focus on type 316L stainless steel because the E_{rp} data are most comprehensive for this alloy. Fig. 1 shows the repassivation potential of 316L stainless steel in chloride-only solutions at three temperatures (23 °C, 60 °C and 95 °C). The model parameters that are necessary to reproduce the results shown in this figure are listed in Table 3. As shown in Fig. 1, the slope of the repassivation potential changes as a function of chloride activity. A steeper slope is observed at low chloride concentrations. This is a general phenomenon for alloys and becomes more pronounced for more corrosion-resistant alloys. The transition between the low-slope and high-slope segments of the curves strongly depends on the alloy and temperature. The less-steep portion of the curve at higher chloride activities is determined by the parameters that represent the dissolution of the metal through the formation of metal-chloride complexes (i.e., $\Delta g^{\neq}_{A,\mathrm{Cl}}$ and n_{Cl}). The steeper portion at lower chloride concentrations is additionally determined by the parameters that represent the formation of the oxide through a reaction with water molecules (i.e., $\Delta g^{\neq}_{I,\mathrm{H_2O}}$ and $\xi_{\mathrm{H_2O}}$). The slope of this segment increases with an increase in the parameter $\xi_{\mathrm{H_2O}}$. Using these parameters, the model represents the data essentially within experimental uncertainty.

In Fig. 1, the repassivation potential is plotted as a function of the activity of chloride ions in the solution. A dependence of E_{rp} on the concentration of the solution, which is more directly measurable than activity, is essentially identical in the dilute solution range (up to ca. 0.1 m) and qualitatively similar for more concentrated solutions. It should be noted that the dependence of E_{rp} on species activity is obtained directly from the repassivation potential model outlined above. However, to calculate the dependence of E_{rp} on concentration, it is necessary to utilize a thermodynamic model for electrolyte solutions. Such a model should relate the concentrations to activities and provide other information such as species distribution and phase equilibria. In this study, we use a previously developed aqueous electrolyte model [19,20] for this purpose. The use of the thermodynamic model in conjunction with the E_{rp} model was described in more detail in a previous paper [7].

Figs. 2–7 show the results of calculations for mixed systems containing chlorides as aggressive species and six different inhibiting ions, i.e., hydroxides, molybdates, vanadates, nitrates, sulfates, and nitrites. In all cases, the results are plotted as a function of inhibitor concentration for fixed chloride concentrations at fixed temperatures. For all inhibitors, calculations have been performed for 23 °C and 60 °C with some additional results for nitrates at 95 °C. In all figures, the experimental data points at higher potentials (above ca. 0.64 V vs. SHE) correspond to experiments in which no localized corrosion was observed. Such data points may correspond to other phenomena such as transpassive dissolution. Therefore, the model is not expected to reproduce such high values exactly at each condition at which they have been obtained. Instead, the model should yield high (although not necessarily the same) values of the repassivation potential at such conditions, thus predicting the absence of localized corrosion. On the other hand, the model is expected to quantitatively reproduce the lower values

Table 3
Parameters of the repassivation potential model and their values for alloys in aqueous chloride–oxyanion environments

Alloy	Species	Model parameters						
		$\Delta g^{\neq}_{A,j}(T_{ref})$ kJ/mol	$\Delta h^{\neq}_{A,j}$ kJ/mol	$n_{A,j}$	$\Delta g^{\neq}_{I,k}(T_{ref})$ kJ/mol	$\Delta h^{\neq}_{I,k}$ kJ/mol	$\xi_{I,k}$	$\Delta G_{ads,j}$ kJ/mol
		Gibbs energy of activation for dissolution mediated by adsorption of aggressive species at reference T	Enthalpy of activation for dissolution mediated by adsorption of aggressive species	Reaction order with respect to aggressive ions	Gibbs energy of activation for formation of oxide mediated by adsorption of inhibitive species at ref. T	Enthalpy of activation for the formation of oxide mediated by adsorption of inhibitive species	Electrochemical transfer coefficient for inhibitive species	Gibbs energy of adsorption
316	H_2O	Not applicable	Not applicable	Not applicable	19.3	0	0.74	10[a]
	Cl^-	−10.9	40	1.46	Not applicable	Not applicable	Not applicable	10[a]
	OH^-	Not applicable	Not applicable	Not applicable	−4.0	−28	0.99[a]	10[a]
	MoO_4^{2-}				−7.4	23	0.99[a]	10[a]
	SO_4^{2-}				−1.1	32	0.99[a]	10[a]
	VO_3^-				−5.0	17	0.99[a]	10[a]
	NO_3^-				15.9	52	0.99[a]	−11
	NO_2^-				14.6	0	0.99[a]	−11
600	H_2O	Not applicable	Not applicable	Not applicable	29.0	−20	0.9	10[a]
	Cl^-	−5.4	74	1.3	Not applicable	Not applicable	Not applicable	10[a]
	OH^-	Not applicable	Not applicable	Not applicable	−2.5	−28	0.99[a]	10[a]
	MoO_4^{2-}				−5.4	23	0.99[a]	10[a]
	SO_4^{2-}				−5.0	18	0.99[a]	10[a]
	VO_3^-				−5.0	18	0.99[a]	10[a]
690	H_2O	Not applicable	Not applicable	Not applicable	19.9	8	0.87	10[a]
	Cl^-	−3.4	78	1.3	Not applicable	Not applicable	Not applicable	10[a]
	OH^-	Not applicable	Not applicable	Not applicable	−1.7	−28	0.99[a]	10[a]
	MoO_4^{2-}				−2.7	23	0.99[a]	10[a]
	SO_4^{2-}				−0.12	32	0.99[a]	10[a]
	VO_3^-				−1.2	18	0.99[a]	10[a]
	NO_3^-				18.2	52	0.99	−11
254SMO	H_2O	Not applicable	Not applicable	Not applicable	27.3	20	0.85	10[a]
	Cl^-	3.4	46	1.3	Not applicable	Not applicable	Not applicable	10[a]
	OH^-	Not applicable	Not applicable	Not applicable	−1.7	−28	0.99[a]	10[a]
	MoO_4^{2-}				−2.2	23	0.99[a]	10[a]
	SO_4^{2-}				−1.3	−60	0.99[a]	10[a]
	NO_3^-				28.1	53	0.99[a]	−11
2205	H_2O	Not applicable	Not applicable	Not applicable	4.9	20	0.9	10[a]
	Cl^-	−7.1	69	1.3	Not applicable	Not applicable	Not applicable	10[a]
	MoO_4^{2-}	Not applicable	Not applicable	Not applicable	−18.5	23	0.99[a]	10[a]
	SO_4^{2-}				−12.6	32	0.99[a]	10v
22	H_2O	Not applicable	Not applicable	Not applicable	−2.2	−19	0.777	10[a]
	Cl^-	8.0	49	1.0	Not applicable	Not applicable	Not applicable	10[a]
	NO_3^-	Not applicable	Not applicable	Not applicable	16.4	50	0.99[a]	−11
s-13Cr	H_2O	Not applicable	Not applicable	Not applicable	2.5	−49	0.74	10[a]
	Cl^-	−21.3	−4.0	1.0	Not applicable	Not applicable	Not applicable	10[a]
	NO_3^-	Not applicable	Not applicable	Not applicable	0.5	52	0.99[a]	−11

[a] Default value, not adjusted using experimental data.

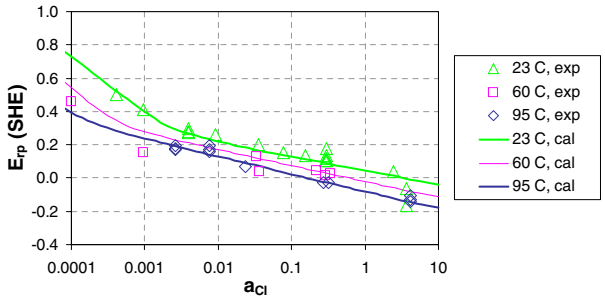

Fig. 1. Repassivation potential of type 316L stainless steel in chloride solutions as a function of chloride ion activity at three temperatures. The symbols denote experimental data reported previously [7] and in the present study. The lines have been obtained from the model.

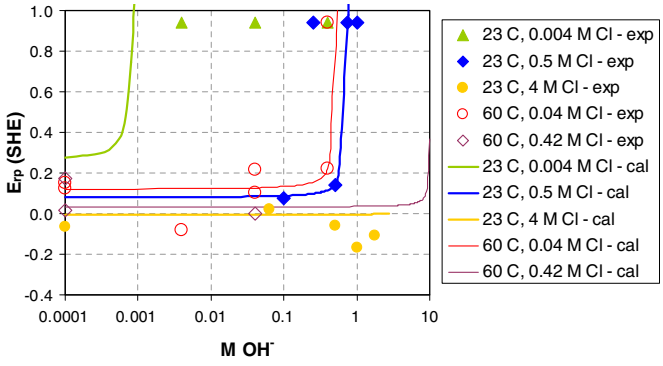

Fig. 2. Calculated and experimental repassivation potentials of type 316L stainless steel in aqueous mixtures containing sodium chloride and hydroxide at 23 °C and 60 °C.

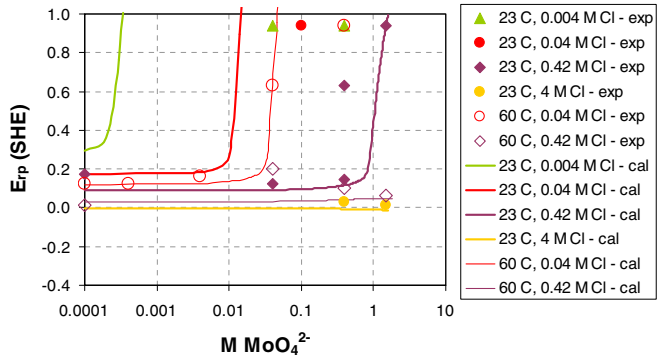

Fig. 3. Calculated and experimental repassivation potentials of type 316L stainless steel in solutions containing sodium chloride and molybdate at 23 °C and 60 °C.

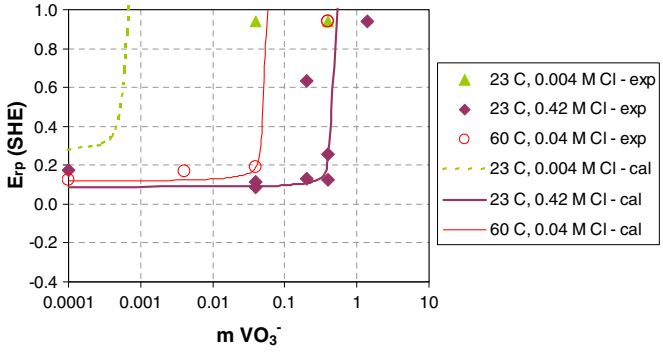

Fig. 4. Calculated and experimental repassivation potentials of type 316L stainless steel in solutions containing sodium chloride and vanadate at 23 °C and 60 °C.

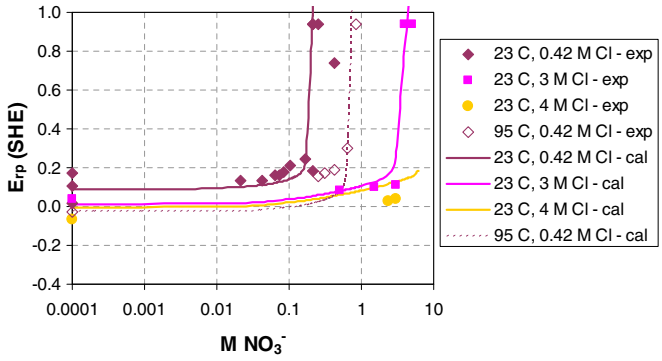

Fig. 5. Calculated and experimental repassivation potentials of type 316L stainless steel in solutions containing sodium chloride and nitrate at 23 °C, 60 °C, and 95 °C.

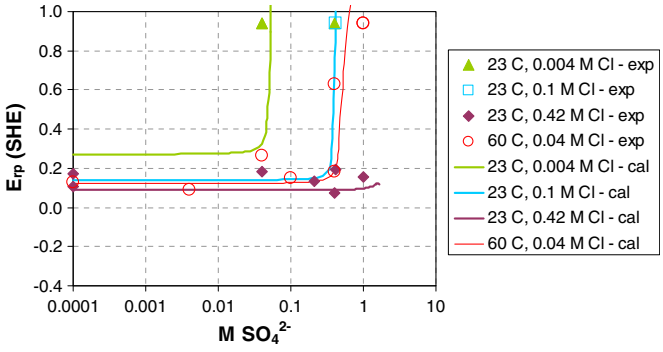

Fig. 6. Calculated and experimental repassivation potentials of type 316L stainless steel in solutions containing sodium chloride and sulfate at 23 °C and 60 °C.

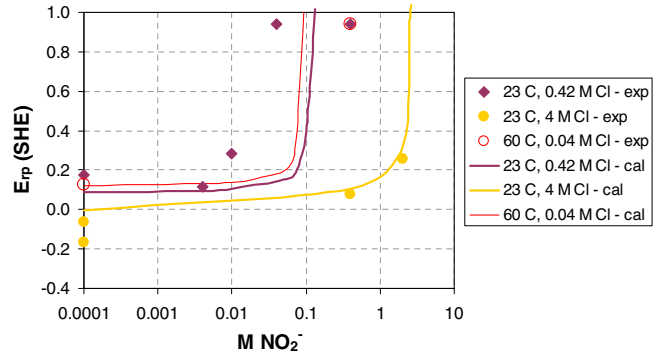

Fig. 7. Calculated and experimental repassivation potentials of type 316L SS in solutions containing sodium chloride and nitrite at 23 °C and 60 °C.

of E_{rp} (i.e., below ca. 0.64 V/SHE), which correspond to the actual occurrence of localized corrosion. The model parameters for the various oxyanions are included in Table 3. As shown in Table 3, the inhibitor effect can be accurately reproduced using only three parameters, i.e., $\Delta g^{\neq}_{I,k}(T_{\mathrm{ref}})$, $\Delta h^{\neq}_{I,k}$, and $\xi_{I,k}$. Of these, only the $\Delta g^{\neq}_{I,k}(T_{\mathrm{ref}})$ and $\Delta h^{\neq}_{I,k}$ parameters are adjusted to match experimental data and $\xi_{I,k}$ is assigned a common value for all inhibitors.

Fig. 2 shows the effect of adding NaOH to NaCl solutions. The E_{rp} vs. OH^- concentration curves have a characteristic shape with two distinct slopes. As the concentration of OH^- ions is increased, the slope of the E_{rp} vs. OH^- concentration curve initially slowly increases with a very low, almost negligible slope. At a certain concentration of OH^-, the slope of the E_{rp} curve rapidly increases and the repassivation potential attains a high value. At OH^-

concentrations that lie beyond the high-slope portion of the E_{rp} vs. OH^- curve, localized corrosion becomes impossible even in systems with a high corrosion potential. Thus, there is a fairly narrow range of OH^- concentrations over which the E_{rp} curve transitions from a low-slope region (in which localized corrosion is possible depending on the value of the corrosion potential) to a high-slope region that constitutes the upper limit of OH^- concentrations for localized corrosion. The exact location of the transition region depends on the temperature and chloride concentration. As shown in Fig. 2, an increase in Cl^- concentration results in a shift in the transition region to higher OH^- concentration. This is due to the fact that more OH^- ions are necessary to inhibit localized corrosion as the concentration of chlorides increases. Similarly, the transition region shifts to higher hydroxide concentrations as the temperature increases. In some cases, inhibition of localized corrosion is impossible because a sufficiently high concentration of inhibiting ions cannot be achieved because of solubility limitations. This is the case for a system containing 4 M NaCl at 23 °C as shown in Fig. 2. For this solution, the E_{rp} vs. OH^- concentration curve terminates at the solubility limit before a transition to a high-slope segment of the curve can be obtained.

Fig. 3 shows the experimental data and results of calculations for mixed systems containing NaCl and Na_2MoO_4. The E_{rp} vs. MoO_4^{2-} concentration curves are qualitatively similar to the E_{rp} vs. OH^- curves in Fig. 2. However, the transition to the inhibition region (i.e., to the steep segment of the curve) occurs at lower inhibitor concentrations. The difference between the MoO_4^{2-} and OH^- ions is quite small at 23 °C, but becomes more pronounced at 60 °C. For example, the transition to the inhibition region for the 0.04 M Cl^- solutions at 60 °C occurs at roughly 0.03 M MoO_4^{2-} and 0.4 M OH^-. This indicates that molybdate ions are more efficient for the inhibition of localized corrosion than hydroxide ions. At some conditions, inhibition cannot be achieved because of solubility limitations. This is shown in Fig. 3 for 4 M Cl^- solutions at 23 °C and 0.42 M Cl^- solutions at 60 °C. For these solutions, the E_{rp} vs. molybdate molarity curve terminates at a point at which the solution becomes saturated with respect to sodium molybdate. Then, the curve cannot transition to a steep segment that would signify inhibition.

The results for vanadate ions are shown in Fig. 4. The effect of vanadates is similar to that of molybdates. In particular, the transition to the inhibition region occurs at similar concentrations for molybdates and vanadates. Fig. 5 shows the experimental data and calculated results for nitrate ions. As shown in Fig. 5, nitrate ions are more efficient as inhibitors of localized corrosion than either molybdate or vanadate ions. This is due to somewhat lower concentrations of nitrate ions that are necessary to achieve the transition to the inhibition region. Also, the relatively high solubility of solids in mixed chloride-nitrate solutions makes it possible to achieve inhibition even for high chloride concentrations. This is illustrated in Fig. 5 for 3 M Cl^- solutions at 23 °C, for which inhibition can be achieved at relatively high nitrate concentrations. However, for 4 M Cl^- solutions, a solubility limit appears just below the transition region to the high-slope segment of the E_{rp} curve.

The Gibbs energy of adsorption ($\Delta G_{ads,i}$) is assigned a constant value for most oxyanions (cf. Table 3). However, the accuracy of representing the E_{rp} data for nitrate solutions is improved if a specific $\Delta G_{ads,\,NO_3}$ value is regressed in addition to the $\Delta g^{\neq}_{I,NO_3}(T_{ref})$ and $\Delta h^{\neq}_{I,NO_3}$ values.

Fig. 6 shows the effect of sulfate ions on the repassivation potential. It is evident that sulfates have an appreciably weaker inhibiting effect than the other ions investigated in this study. For example, the sulfate concentration that is necessary to inhibit localized corrosion in 0.04 M Cl^- solutions at 60 °C is approximately 0.4 M and is about an order of magnitude higher than the necessary concentration of molybdates, vanadates or nitrates. Also, solubility limits are encountered at relatively low concentrations, e.g., 0.42 M Cl^- solutions cannot be inhibited at 23 °C due to a solubility limit.

Fig. 7 illustrates the inhibiting behavior of nitrites. It is evident that nitrites have somewhat stronger inhibitive properties than nitrates. In particular, inhibition in 4 M Cl^- solutions can be achieved at 23 °C because the transition to the inhibition range is not prevented by solubility limits.

Figs. 8–12 show the repassivation potential of alloy 600 in various environments. Fig. 8 compares the calculated E_{rp} values with experimental data for chloride-only environments. The data are less comprehensive for alloy 600 than for 316L SS, but they are sufficient to establish model parameters. Figs. 9–12 show the effect of hydroxide, molybdate, vanadate, and sulfate ions, respectively. The general patterns are similar to those observed for 316L SS. In par-

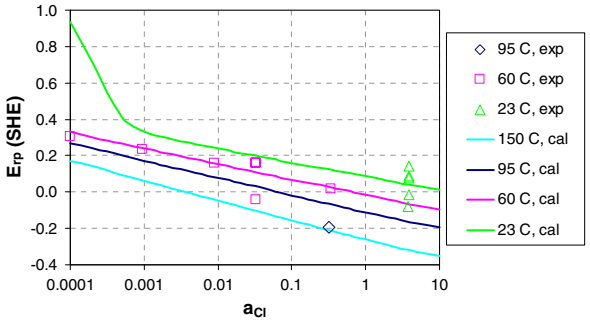

Fig. 8. Repassivation potential of alloy 600 as a function of chloride activity at various temperatures.

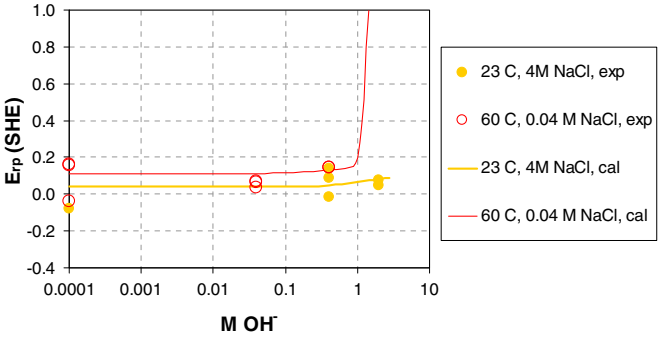

Fig. 9. Calculated and experimental repassivation potentials of alloy 600 in mixed chloride–hydroxide solutions at 23 °C and 60 °C.

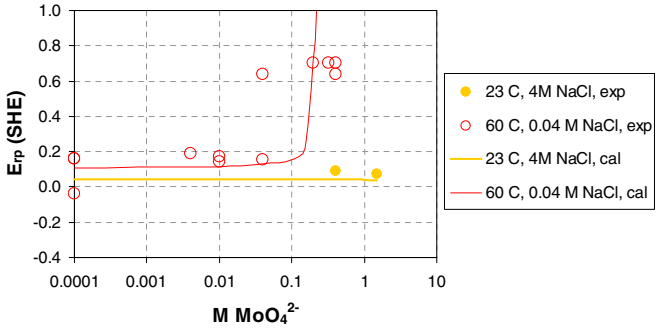

Fig. 10. Calculated and experimental repassivation potentials of alloy 600 in mixed chloride–molybdate solutions at 23 °C and 60 °C.

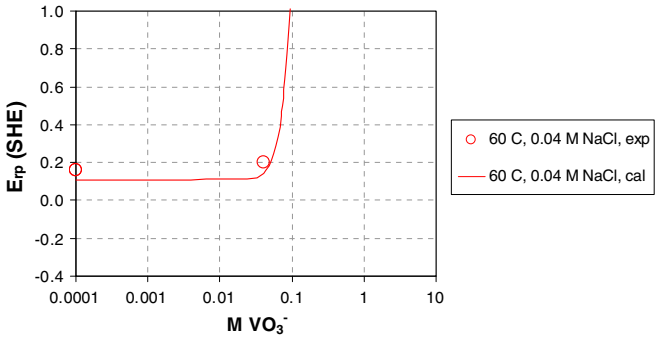

Fig. 11. Calculated and experimental repassivation potentials of alloy 600 in mixed chloride–vanadate solutions at 60 °C.

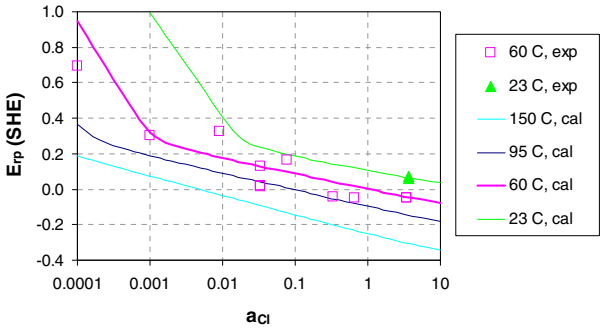

Fig. 13. Repassivation potential of alloy 690 as a function of chloride activity and temperature.

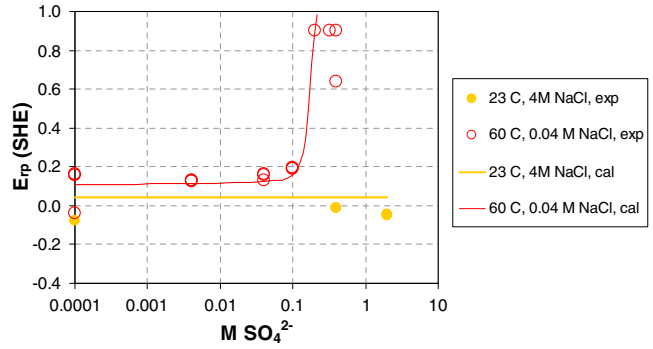

Fig. 12. Calculated and experimental repassivation potentials of alloy 600 in mixed chloride-sulfate solutions at 23 °C and 60 °C.

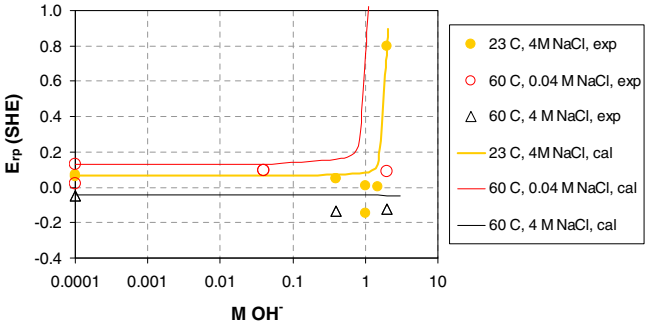

Fig. 14. Calculated and experimental repassivation potentials of alloy 690 in mixed chloride–hydroxide solutions at 23 °C and 60 °C.

ticular, the transition from the region in which localized corrosion is possible to the inhibition region occurs at similar oxyanion concentrations as long as the temperature and chloride ion concentration are the same. The critical oxyanion concentration for the transition differs by a factor of 2–4 between the two alloys. When compared with 316L SS, the critical oxyanion concentrations are higher for alloy 600 in the case of the OH^-, MoO_4^{2-}, and VO_3^- ions, but somewhat lower in the case of the SO_4^{2-} ions.

It can be observed that a few experimental E_{rp} values seem to be somewhat lower at higher oxyanion concentrations than in chloride-only solutions. This is the case for 316L SS in hydroxide solutions (Fig. 2) and for alloy 600 in sulfate solutions. The model does not reproduce this occasional depression in the E_{rp} values. In principle, such behavior could be accounted for only by a very substantial increase in the activity coefficients of Cl^- ions in chloride–oxyanion mixtures at high concentrations, which would increase the activity of chloride ions and, hence, depress the repassivation potential. However, it seems more plausible to attribute this observation to the scattering of experimental data because it occurs only for a few alloy–oxyanion combinations and does not have a general character.

Figs. 13–18 summarize the calculated and experimental repassivation potentials for alloy 690. The E_{rp} values for alloy 690 are somewhat higher than those for alloy 600, especially at low chloride activities (cf. Fig. 13). This is due to the higher Cr content of alloy 690, which can be expected to contribute to the resistance to localized corrosion. The transition from the localized corrosion to the inhibition region occurs at similar oxyanion concentrations as for alloy 600. However, the higher resistance of alloy 690 to localized corrosion makes it possible to achieve inhibition at somewhat higher Cl^- concentrations, where no inhibition is possible for alloy 600. This is illustrated in Fig. 14, which shows a transition to

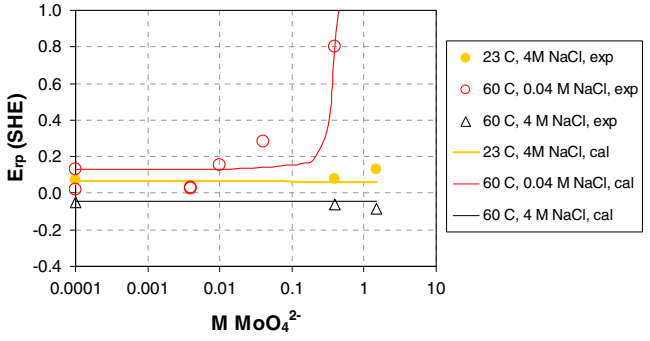

Fig. 15. Calculated and experimental repassivation potentials of alloy 690 in mixed chloride–molybdate solutions at 23 °C and 60 °C.

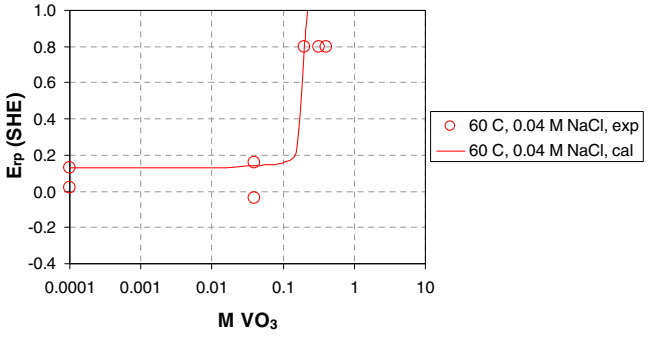

Fig. 16. Calculated and experimental repassivation potentials of alloy 690 in mixed chloride–vanadate solutions at 23 °C and 60 °C.

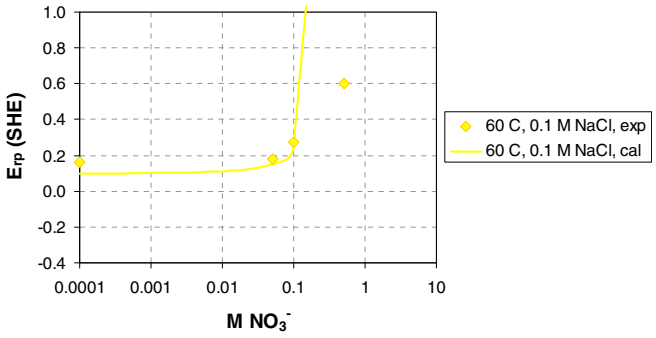

Fig. 17. Calculated and experimental repassivation potentials of alloy 690 in mixed chloride–nitrate solutions at 60 °C.

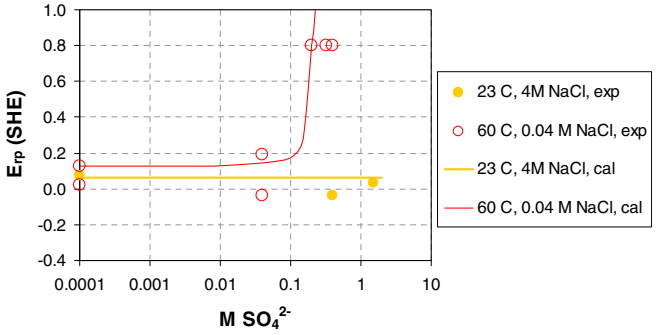

Fig. 18. Calculated and experimental repassivation potentials of alloy 690 in mixed chloride–sulfate solutions at 23 °C and 60 °C.

inhibition in a 4 M Cl solution at high concentrations of OH^- ions. In the case of alloy 600, such a transition does not occur before the saturation limit is reached (cf. Fig. 9).

Figs. 19–22 illustrate the effect of chlorides and oxyanions on the repassivation potential of alloy 254SMO. As shown in Fig. 19, the E_{rp} values of alloy 254SMO are substantially higher at all chloride activities than those of alloys 600 and 690 or type 316L stainless steel. This is due to the Mo and N content of alloy 254SMO, which contributes to the resistance to localized corrosion. Also, the enhanced resistance to localized corrosion manifests itself in a more pronounced high-slope segment of the E_{rp} vs. chloride activity curve at low chloride activities. Because of the higher resistance of alloy 254SMO to localized corrosion, lower concentrations of oxyanions are necessary for a transition to the inhibition range. For example, the critical concentration of MoO_4^{2-} ions that is necessary to achieve inhibition is lower for 0.4 M Cl^- solutions at 60 °C (cf. Fig. 20) than that needed for alloy 690 in 0.04 M Cl^- solutions at the same temperature.

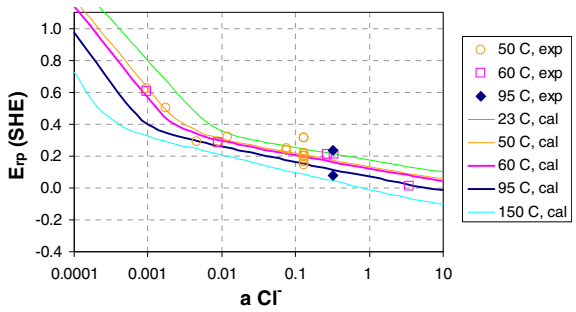

Fig. 19. Repassivation potential of alloy 254SMO as a function of chloride activity and temperature. The experimental data are from this study and Sridhar et al. [8].

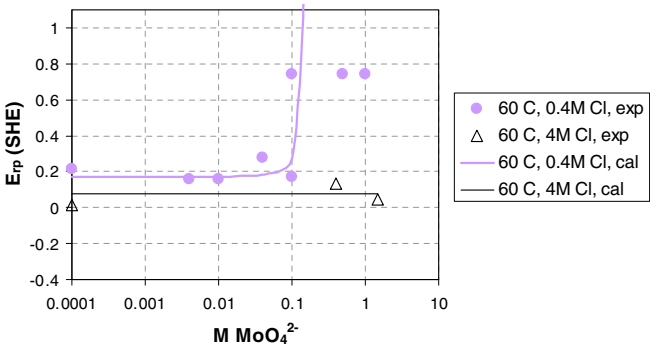

Fig. 20. Calculated and experimental repassivation potentials of alloy 254SMO in mixed chloride–molybdate solutions at 60 °C.

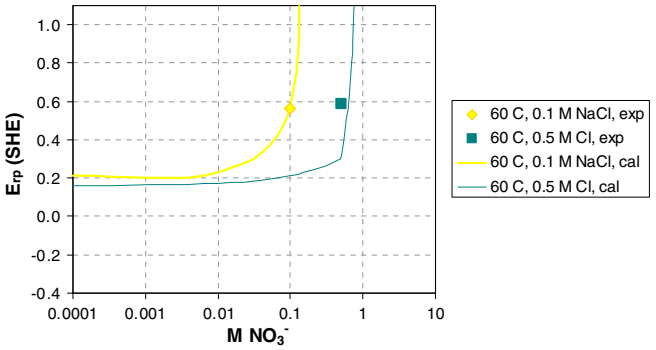

Fig. 21. Calculated and experimental repassivation potentials of alloy 254SMO in mixed chloride–nitrate solutions at 60 °C.

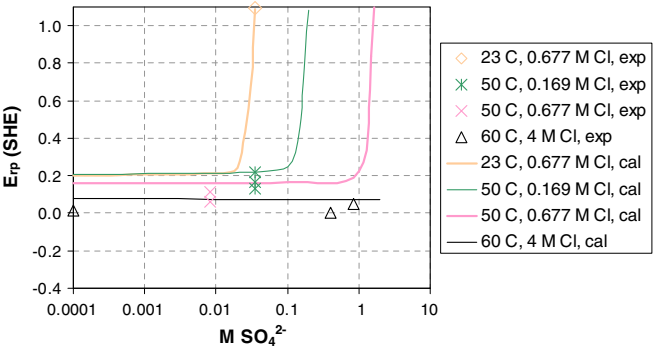

Fig. 22. Calculated and experimental repassivation potentials of alloy 254SMO in mixed chloride–sulfate solutions.

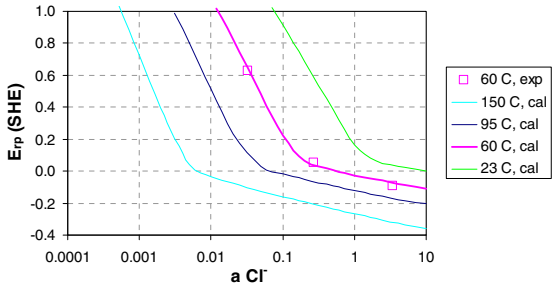

Fig. 23. Repassivation potential of type 2205 duplex stainless steel as a function of chloride activity.

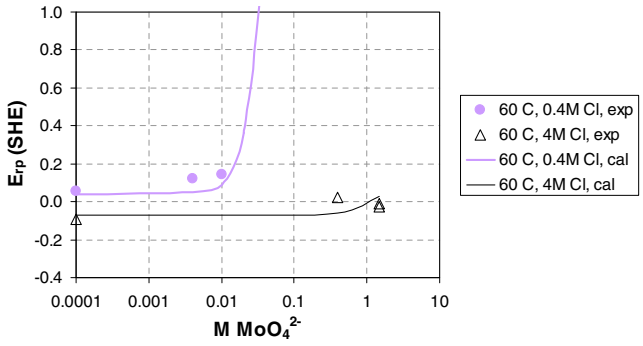

Fig. 24. Calculated and experimental repassivation potentials of type 2205 stainless steel in mixed chloride–molybdate solutions.

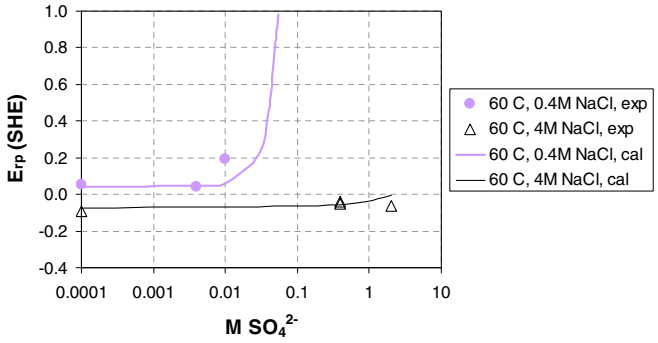

Fig. 25. Calculated and experimental repassivation potentials of type 2205 stainless steel in mixed chloride–sulfate solutions.

Figs. 23–25 summarize the repassivation potentials for the 2205 duplex stainless steel. Fig. 23 indicates that the behavior of E_{rp} as a function of chloride activity is substantially different from that observed for the other alloys. While the repassivation potential is fairly low and similar to that for alloys 316L or 600 at higher Cl^- activities, it is substantially higher in more dilute chloride solutions. This results in a very pronounced high-slope segment of the E_{rp} vs. chloride activity plot. Although there is only one experimental point that proves the existence of the high-slope segment here, the shape of the E_{rp} curve in Fig. 23 is supported by the generalized correlation for calculating E_{rp} in terms of alloy composition (cf. Section 4.3). Figs. 24 and 25 show the effect of molybdate and sulfate ions, respectively. The oxyanion concentration that is necessary for the transition to the inhibition range is similar to that observed for alloy 254SMO.

In the case of alloy 22, the analysis has been performed on the basis of previously published data [7,16,17]. The experimental E_{rp} data for this alloy are particularly comprehensive and cover the range from 313 K to 448 K as shown in Fig. 26. Due to its high Mo and W content, alloy 22 has the highest resistance to localized corrosion among the alloys studied here. This leads to substantially higher E_{rp} values, most of which lie on the high-slope segment of the E_{rp} vs. chloride activity diagram. This is in contrast with the alloys containing lower concentrations of Mo and W, for which the low-slope segment covers most of the practically important chloride activity (or concentration) range and the high-slope segment extends only over dilute solutions. For this alloy, the experimental data on the effect of oxyanions are limited to nitrates. The effect of nitrates on the repassivation potential is shown in Fig. 27 for temperatures ranging from 353 K to 383 K. As a result of the high resistance of alloy 22 to localized corrosion, inhibition can be achieved even at elevated temperatures in concentrated chloride solutions (e.g., 4 M NaCl and 4 M $MgCl_2$ in Fig. 27).

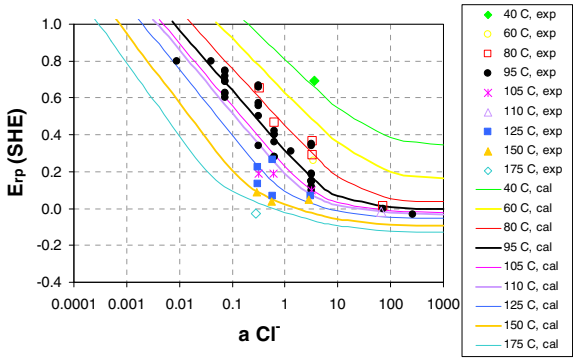

Fig. 26. Repassivation potential of alloy 22 as a function of chloride activity and temperature. The experimental data are from Dunn et al. [16,17] and Anderko et al. [7].

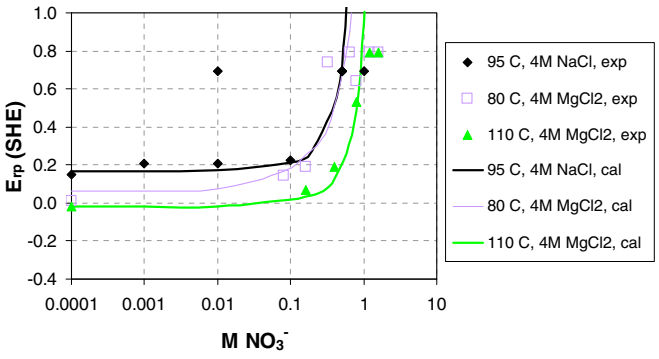

Fig. 27. Calculated and experimental repassivation potential of alloy 22 in mixed chloride–nitrate solutions at 80 °C, 95 °C, and 110 °C. The experimental data are from Dunn et al. [16,17].

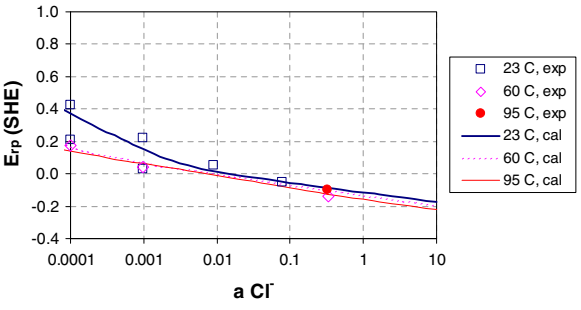

Fig. 28. Repassivation potential of S-13Cr stainless steel (UNS 41425) as a function of chloride activity and temperature.

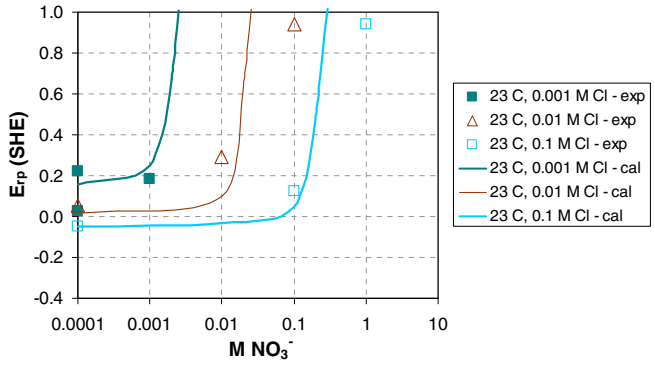

Fig. 29. Calculated and experimental repassivation potentials of S-13Cr stainless steel (UNS 41425) in mixed chloride–nitrate solutions at 23 °C.

Finally, Figs. 28 and 29 show the repassivation potentials of S-13Cr stainless steel in chloride and chloride-nitrate solutions. This martensitic stainless steel has the lowest resistance to localized corrosion among the alloys studied here due to its relatively low Cr content. This is evident from the relatively low values of E_{rp} in Fig. 28, which are below those for 316L SS (Fig. 1) and alloy 600 (Fig. 8). As shown in Fig. 29, nitrates inhibit localized corrosion of this alloy in relatively dilute chloride solutions.

The parameters established in this study have been determined based on individual chloride-oxyanion combinations and multicomponent systems have not been investigated. However, it has been shown in our previous studies [7,11] that the repassivation model can accurately predict E_{rp} in complex, multicomponent solutions as long as the parameters for oxyanions are derived from individual data. Therefore, complex systems were not studied here.

For all the investigated alloy–chloride–oxyanion combinations, the model reproduces the experimental data essentially within experimental uncertainty. The strong regularities that are observed in the repassivation behavior of various alloys, coupled with the evident qualitative relationship between the E_{rp} values and the amount of alloying elements, indicate that a generalized correlation can be established for calculating the repassivation potential as a function of alloy composition.

4.3. Generalization of the model as a function of alloy composition

It is well known that the resistance of stainless steels and nickel-base alloys to localized corrosion can be correlated with the concentrations of Cr, Mo, W, and N in the alloy. On the empirical level, the Pitting Resistance Equivalence (PRE) has been extensively used to rank the relative performance of alloys in aggressive environments. The PRE indices have been developed using a number of empirically derived equivalent compositions [21]. These alloy equivalents are limited to the experimental conditions and the range of alloys considered [22]. The effect of alloying elements, especially chromium and molybdenum, has also been extensively studied from a mechanistic point of view [23–26]. Essentially two types of approaches have been tried: those based on the effect of alloying elements on the passive film behavior and those that are based on the effect of the alloying components on the kinetics of dissolution in a nascent pit electrolyte. Urquidi-Macdonald and Macdonald [26], using the point defect model formalism, suggested that the role of alloying elements, such as Mo and W, is in modifying the concentration and diffusivity of cation vacancies in the passive film. The higher cationic charges of Mo and W compared to Ni and Cr in the passive film act as a "trap" for the cation vacancies and thus reduce their rate of condensation at the film-metal interface, which is considered to be the precursor for pitting. Laycock and Newman [27] suggested that the role of Mo in increasing an alloy's resistance to localized corrosion is due to reducing the dissolution kinetics of the metal in the acidic, concentrated chloride solution present in a nascent pit. Tungsten can be expected to play a similar role. Although Mo and W may increase localized corrosion resistance through their effect on pit nucleation, there is evidence that molybdenum is responsible for repassivation after breakdown occurs. Repassivation potential increases with the amount of molybdenum in the alloy [25]. Also, it is generally accepted that the addition of nitrogen improves resistance to localized corrosion [28–30]. The dominant effect of nitrogen is associated with repassivation and has been attributed variously to the accumulation of nitrogen on the surface [28], which alters the kinetics of dissolution in the nascent pit or crevice electrolyte, or to the formation of surface nitrides [31]. Similarly, the effect of inhibitive ions on pit initiation has been discussed either in terms of their effect on the adsorption of chlorides on the passive film or the transport of chlorides in the pit electrolyte or on the lacy covers on pits. Towards the last aspect, it has also been argued [32] that some "inhibitors" such as sulfate may also act as aggressive agents.

In this study, it is not our objective to examine the relationship between the repassivation potential and alloy composition or inhibitive species from a mechanistic point of view. Rather, we use the available E_{rp} database to establish an empirical correlation for calculating the repassivation potential as a function of alloy composition. The purpose of such a correlation is to predict the repassivation potential for alloys for which experimental data are not available or are uncertain. At the same time, the relative numerical significance of terms associated with various alloying elements can contribute to our understanding of the importance of these elements in the repassivation process. In a previous study [33], a preliminary version of such a correlation was shown to be promising for a number of alloys in chloride solutions. Here, we develop a much more accurate and comprehensive correlation using a larger database. Further, we extend it to systems that contain oxyanions in addition to chlorides.

In the first step, a correlation has been established for Fe–Ni–Cr–Mo–W–N alloys in chloride-only solutions. This correlation is based on a database containing E_{rp} values for 15 metals. In addition to the alloys discussed above (i.e., 316L, 600, 690, 254SMO, 2205, 22, and S-13Cr), the database contains E_{rp} data collected in Table 2 for alloys 625, 276, AL6XN, and 800 and previously published data for alloy 825 [34,7], 304L stainless steel [35], carbon steel [36], and nickel [37,38].

As shown in Table 3, the repassivation potential of an alloy in an environment containing water and chloride ions is characterized, in the most general case, by seven parameters, i.e., $\Delta g^{\neq}_{A,Cl}(T_{ref})$, $\Delta h^{\neq}_{A,Cl}$, $n_{A,Cl}$, $\Delta g^{\neq}_{I,H_2O}(T_{ref})$, $\Delta h^{\neq}_{I,H_2O}$, ξ_{I,H_2O}, and $\Delta G_{ads,Cl}$. The parameters $\Delta g^{\neq}_{A,Cl}(T_{ref})$, $\Delta h^{\neq}_{A,Cl}$, $n_{A,Cl}$, ξ_{I,H_2O}, and $\Delta G_{ads,Cl}$ are specific to the effect of chloride ions whereas the parameters $\Delta g^{\neq}_{I,H_2O}(T_{ref})$, $\Delta h^{\neq}_{I,H_2O}$, and $\xi_{I,H2O}$ remain independent of the ionic species in the solution. This seemingly large number of parameters is not a hindrance to the development of a general treatment because the parameters show significant regularities. In particular, three parameters can be assigned universal values without any appreciable loss in accuracy. Specifically, the Gibbs energy of adsorption of ions can be set equal to a common value, i.e.

$$\Delta G_{ads,Cl}/(kJ/mol) = 10 \tag{8}$$

Further, analysis of experimental data reveals that the steeper portions of the plots of E_{rp} vs. chloride activity have similar slopes for various alloys. These slopes are controlled by the electrochemical transfer coefficient for the formation of passive oxide as a result of a reaction with water (ξ_{I,H_2O}). Thus, the ξ_{I,H_2O} parameter can be assigned a common value, i.e.

$$\xi_{I,H_2O} = 0.8 \tag{9}$$

The slopes of the less-steep segments of the E_{rp} vs. Cl^- activity plots are also reasonably similar. These slopes are controlled by the $n_{A,Cl}$ parameter, which can be thus given a constant value, i.e.

$$n_{A,Cl} = 1.1 \tag{10}$$

Further analysis reveals that the enthalpies of activation $\Delta h^{\neq}_{A,Cl}$ and $\Delta h^{\neq}_{I,H_2O}$ are linearly related to the respective Gibbs energies of activation $\Delta g^{\neq}_{A,Cl}(T_{ref})$ and $\Delta g^{\neq}_{I,H_2O}(T_{ref})$. Such linear relations are not unexpected because analogous regularities are commonly observed for the enthalpies and Gibbs energies of formation of species that belong to homologous series. These relationships are given by

$$\Delta h^{\neq}_{A,Cl} = 55 + 2\Delta g^{\neq}_{A,Cl}(T_{ref}) \tag{11}$$

$$\Delta h^{\neq}_{I,H_2O} = -15 + 32\Delta g^{\neq}_{I,H_2O}(T_{ref}) \tag{12}$$

This leaves only the two Gibbs energies of activation $\Delta g^{\neq}_{A,Cl}(T_{ref})$ and $\Delta g^{\neq}_{I,H_2O}(T_{ref})$ to be determined explicitly in terms of alloy composi-

tion. Since the Gibbs energies of activation are thermodynamic quantities, their dependence on composition can be formally expressed by accounting for binary pair-wise contributions of components (cf. [39])

$$\Delta g^{\neq} = \sum_{i}^{N}\sum_{j}^{N} w_i w_j a_{ij} \tag{13}$$

where w_i ($i = 1,\ldots,N$) is the fraction of component i and a_{ij} are empirical binary parameters. Here, we define w_i as weight fractions. In practice, it is not feasible to account independently for all binary terms because the database would not be sufficiently large for such a purpose. Therefore, some terms need to be neglected while others are grouped and appropriate exponents are introduced on an empirical basis.

To calculate the Gibbs energy of activation for dissolution mediated by adsorption of aggressive species ($\Delta g^{\neq}_{A,\mathrm{Cl}}(T_{\mathrm{ref}})$), four contributions are needed, i.e.,

$$\Delta g^{\neq}_{A,\mathrm{Cl}}(T_{\mathrm{ref}}) = \Delta g^{\neq}_{A,\mathrm{Cl}}(\mathrm{Cr,Fe,Ni}) + \Delta g^{\neq}_{A,\mathrm{Cl}}(\mathrm{Mo,W}) + \Delta g^{\neq}_{A,\mathrm{Cl}}(N) + \Delta g^{\neq}_{A,\mathrm{Cl}}(\mathrm{misc}) \tag{14}$$

where $\Delta g^{\neq}_{A,\mathrm{Cl}}(\mathrm{Cr,Fe,Ni})$ is the baseline contribution for Fe–Ni–Cr alloys, $\Delta g^{\neq}_{A,\mathrm{Cl}}(\mathrm{Mo,W})$ is an increment due to the effect of Mo and W, $\Delta g^{\neq}_{A,\mathrm{Cl}}(N)$ is an increment due to N and $\Delta g^{\neq}_{A,\mathrm{Cl}}(\mathrm{misc})$ is a miscellaneous contribution of other elements. The baseline contribution for Fe–Ni–Cr alloys reproduces the Gibbs energy of activation, $\Delta g^{\neq}_{A,\mathrm{Cl}}(T_{\mathrm{ref}})$, for alloys 600, 690, 800, and 304L as well as for carbon steel and nickel. It is given by:

$$\Delta g^{\neq}_{A,\mathrm{Cl}}(\mathrm{Cr,Fe,Ni}) = \Delta g^{\neq}_{A,\mathrm{Cl}}(\mathrm{Fe})w_{\mathrm{Fe}} + \Delta g^{\neq}_{A,\mathrm{Cl}}(\mathrm{Ni})w_{\mathrm{Ni}} + 398.5 w_{\mathrm{Cr}} w_{\mathrm{Ni}}^{0.7} + 555.9 w_{\mathrm{Cr}} w_{\mathrm{Fe}}^{0.7} - 335.4 w_{\mathrm{Cr}} \tag{15}$$

where $\Delta g^{\neq}_{A,\mathrm{Cl}}(\mathrm{Fe}) = -74.1$ and $\Delta g^{\neq}_{A,\mathrm{Cl}}(\mathrm{Ni}) = -18.7$ are the Gibbs energies of activation for iron (or, for practical purposes, carbon steel) and nickel, respectively. The remaining contributions are calculated as

$$\Delta g^{\neq}_{A,\mathrm{Cl}}(\mathrm{Mo,W}) = w_{\mathrm{Cr}}(w_{\mathrm{Mo}} + w_{\mathrm{W}})^{0.4}(893.9 w_{\mathrm{Ni}}^{1.7} + 839.0 w_{\mathrm{Fe}}^{1.7}) \tag{16}$$

$$\Delta g^{\neq}_{A,\mathrm{Cl}}(N) = w_N^{0.5} w_{\mathrm{Cr}}^{3}[-1.293e5 w_{\mathrm{Fe}}^{0.2} + 1.451e5 w_{\mathrm{Ni}}^{0.2})] \tag{17}$$

$$\Delta g^{\neq}_{A,\mathrm{Cl}}(\mathrm{misc}) = -1764 w_{\mathrm{Nb}} w_{\mathrm{Cr}} \tag{18}$$

With the currently available database, the $\Delta g^{\neq}_{A,\mathrm{Cl}}(\mathrm{misc})$ term is limited to the effect of Nb.

A similar scheme is adopted for the Gibbs energy of activation for the formation of oxide mediated by adsorption of H_2O, i.e.,

$$\Delta g^{\neq}_{I,\mathrm{H_2O}}(T_{\mathrm{ref}}) = \Delta g^{\neq}_{I,\mathrm{H_2O}}(\mathrm{Cr,Fe,Ni}) + \Delta g^{\neq}_{I,\mathrm{H_2O}}(\mathrm{Mo,}W) + \Delta g^{\neq}_{I,\mathrm{H_2O}}(N) + \Delta g^{\neq}_{I,\mathrm{H_2O}}(\mathrm{misc}) \tag{19}$$

where

$$\Delta g^{\neq}_{I,\mathrm{H_2O}}(\mathrm{Cr,Fe,Ni}) = 18.14 w_{\mathrm{Fe}} + 169.6 w_{\mathrm{Ni}} + 1983 w_{\mathrm{Cr}}^{1.1} \tag{20}$$

$$\Delta g^{\neq}_{I,\mathrm{H_2O}}(\mathrm{Mo,W}) = -2422[(w_{\mathrm{Mo}} + w_{\mathrm{W}})^{1.1} + w_{\mathrm{Cr}}^{1.1}(w_{\mathrm{Fe}} + 1.4 w_{\mathrm{Ni}})] + 2024[(w_{\mathrm{Mo}} + w_{\mathrm{W}})^{1.1}(w_{\mathrm{Fe}}^{0.5} + w_{\mathrm{Ni}}^{0.5})] \tag{21}$$

$$\Delta g^{\neq}_{I,\mathrm{H_2O}}(N) = w_N^{0.5} w_{\mathrm{Cr}}^{3}[-2.607 d5 w_{\mathrm{Fe}}^{0.2} + 2.384 e5 w_{\mathrm{Ni}}^{0.2}] \tag{22}$$

$$\Delta g^{\neq}_{I,\mathrm{H_2O}}(\mathrm{misc}) = -4950 w_{\mathrm{Nb}} w_{\mathrm{Cr}} \tag{23}$$

The coefficients of Eqs. (15) and (19) were determined by simultaneously regressing E_{rp} data for Fe–Ni–Cr alloys (i.e., those that do not contain Mo, W, N, or Nb) in chloride solutions as a function of chloride concentration and temperature. This regression included nickel and iron (approximated by carbon steel) as limiting cases. In the regressions, Eqs. (9)–(12) were used as constraints. After determining the coefficients of Eqs. (15) and (19), the coefficients of Eqs. (16) and (21) were regressed using the E_{rp} data for the alloys that contain Mo and W in addition to Cr, but do not contain N or Nb. Then, Eqs. (17) and (22) were established using the data for the alloys that contain N in addition to Cr, Mo, and W (i.e., alloys 254SMO, AL6XN and 2205). Finally, the coefficients of Eqs. (18) and (23) were regressed using the E_{rp} data for alloy 625. Since Eqs. (18) and (23) are based on data for a single alloy, they should be treated as tentative.

Thus, Eqs. (8)–(12) and (14)–(23) constitute a generalized correlation for predicting E_{rp} of Fe–Ni–Cr–Mo–W–N alloys as a function

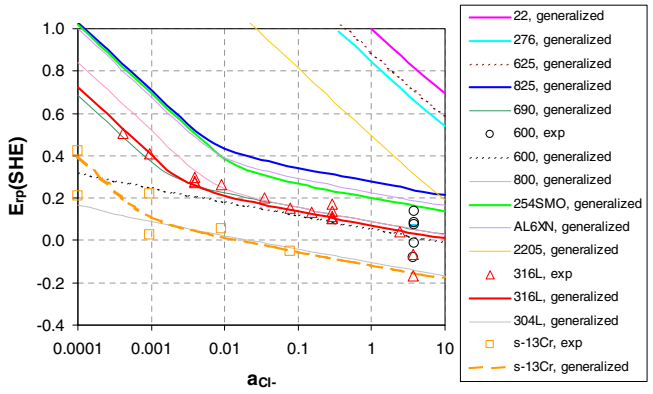

Fig. 30. Comparison of repassivation potential values obtained from the generalized correlation with alloy composition (Eqs. (8)–(12) and (14)–(23)) with experimental data for various alloys at 23 °C.

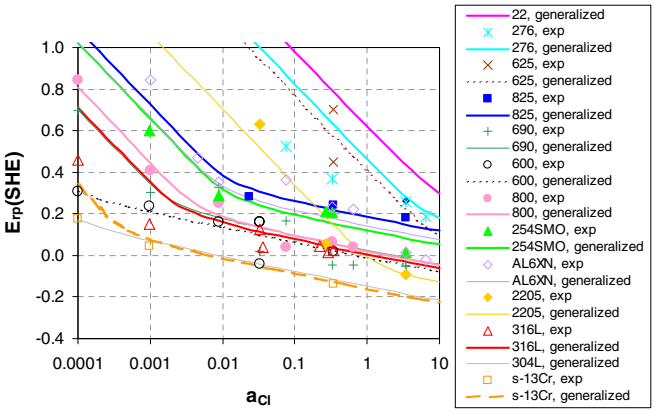

Fig. 31. Comparison of E_{rp} values obtained from the generalized correlation (Eqs. (8)–(12) and (14)–(23)) with experimental data for various alloys at 60 °C.

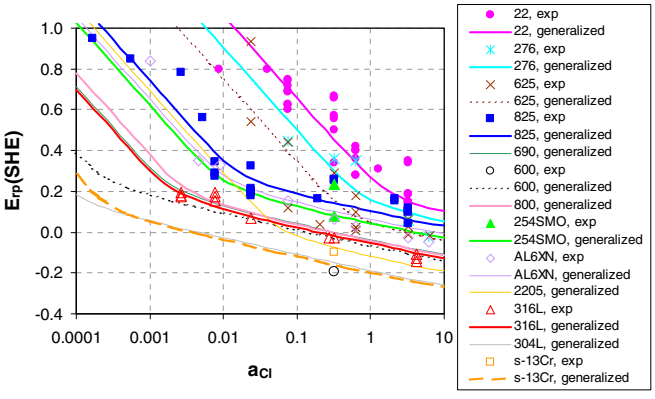

Fig. 32. Comparison of E_{rp} values obtained from the generalized correlation (Eqs. (8)–(12) and (14)–(23)) with experimental data for various alloys at 95 °C.

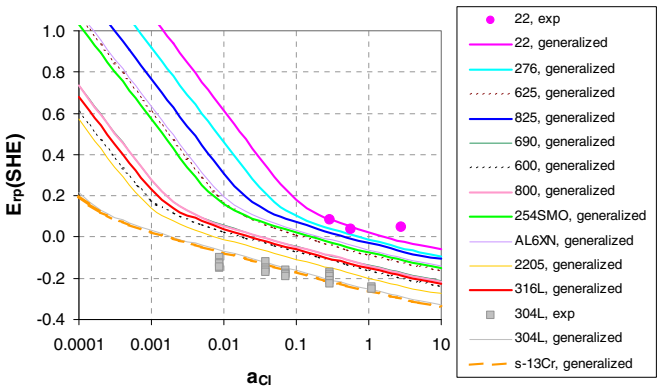

Fig. 33. Comparison of E_{rp} values obtained from the generalized correlation (Eqs. (8)–(12) and (14)–(23)) with experimental data for various alloys at 150 °C.

of composition. The repassivation potentials calculated from this correlation are shown in Figs. 30–33 for 13 alloys in chloride solutions at 296 K, 333 K, 368 K and 423 K, respectively. The calculated curves are in generally good agreement with experimental data. The overall average deviation between the calculated results and experimental data for all alloys is 67 mV. This can be compared with the average deviation of 56 mV, which is obtained when repassivation potential data are fitted separately for each alloy. Thus, the generalized correlation increases the overall deviation only from 56 to 67 mV. Since Figs. 30–33 compare the repassivation potentials of various alloys, they can also be used for ranking the alloys with respect to their resistance to localized corrosion as a function of chloride activity and temperature.

4.4. Generalization of the model for mixed chloride–oxyanion environments

The generalized correlation can be extended to mixed systems containing chlorides and oxyanions. For this purpose, we note that there is a relationship between the Gibbs energy of activation for the formation of oxide due to the adsorption of oxyanions (i.e., $\Delta g^{\neq}_{I,k}$ with $k = OH^-, MoO_4^{2-}, VO_3^-, SO_4^{2-}, NO_3^-$) and that due to the adsorption of H_2O (i.e., $\Delta g^{\neq}_{I,H_2O}$). This relationship is shown in Fig. 34. The symbols in Fig. 34 correspond to the seven alloys for which the anion effects were investigated (i.e., 316L, 600, 690, 254SMO, 2205, 22, and s-13Cr). The existence of such a relationship is understandable considering the fact that the tendency for repassivation in oxyanion-containing environments can be expected to be qualitatively related to that in oxyanion-free solutions. The relationship shown in Fig. 34 can be expressed as

$$\Delta g^{\neq}_{I,k}(T_{ref}) = \min[(q_1 \Delta g^{\neq}_{I,H_2O}(T_{ref}) + q_2), (q_3 \Delta g^{\neq}_{I,H_2O}(T_{ref}) + q_4)] \quad (24)$$

where the coefficients q_i ($i = 1 \ldots, 4$) are listed in Table 4 for the five investigated anions. Also, Table 4 includes the values of the enthalpy of activation $\Delta h^{\neq}_{I,k}$ and electrochemical transfer coefficient ξ_k, which can be assigned constant values for various alloys. The dashed diagonal line in Fig. 34 shows a hypothetical line at which $\Delta g^{\neq}_{I,k} = \Delta g^{\neq}_{I,H_2O}$. The $\Delta g^{\neq}_{I,k}$ values for the inhibitors lie below the diagonal line, thus indicating that the effect of the inhibiting ions is stronger than that of H_2O (i.e., $\Delta g^{\neq}_{I,k} < \Delta g^{\neq}_{I,H_2O}$). Once $\Delta g^{\neq}_{I,H_2O}$ is calculated from Eqs. (19)–(23) as a function of alloy composition, Eq. (24) can be used to predict the $\Delta g^{\neq}_{I,k}$ values for the anions. It is noteworthy that the $\Delta g^{\neq}_{I,k}$ values are quite similar for the OH^-, MoO_4^{2-}, VO_3^-, and SO_4^{2-} anions. Thus, the main difference in the effect of these anions lies in their thermodynamic properties (as exemplified by their solubilities) and, once the thermodynamic effects are factored out, the contributions of these anions to repassivation are similar. On the other hand, the effect of nitrates is substantially different.

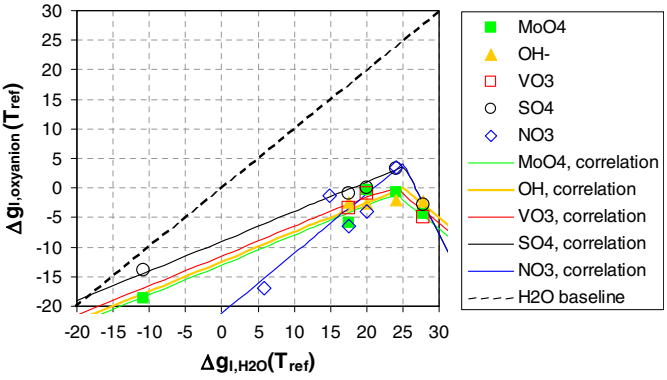

Fig. 34. Correlation between the Gibbs energy of activation for the formation of oxide mediated by adsorption of various oxyanions $[\Delta g^{\neq}_{I,oxyanion}(T_{ref})]$ and that due to the adsorption of water $[\Delta g^{\neq}_{I,H_2O}(T_{ref})]$ (Eq. 24 and Table 4).

Table 4
Parameters for calculating the Gibbs energy and enthalpy of activation for the formation of oxide mediated by the adsorption of inhibitive species as a function of alloy concentration (Eq. 24)

Species (k)	$\Delta g_{I,k}(T_{ref})$ correlation				$\Delta h_{I,k}$	$\xi_{I,k}$	$\Delta G_{ads,k}$
	q_1	q_2	q_3	q_4			
OH^-	0.5	−12.5	−1	25	−6	0.99	10
MoO_4^{2-}	0.5	−13	−1	23	44	0.99	10
SO_4^{2-}	0.5	−9	−2.5	67	32	0.99	10
VO_3^- [a]	0.5	−11.5	−1	24	18	0.99	10
NO_3^-	1	−21	−2.5	67	32	0.99	10

[a] Includes hydrolyzed species, i.e., $H_2VO_4^-, HVO_4^{2-}$.

With the currently available database, the relationship shown in Fig. 34 and expressed by Eq. (24) should be treated as tentative. The existence of the two linear functions (which give an inverse "V" shape) is based on a fairly limited amount of information and would need to be further confirmed using additional data, especially in the negative slope region. Nevertheless, the relationship depicted in Fig. 34 provides a convenient way of systematizing the parameters that have been obtained for various alloy-oxyanion combinations.

It must be noted that the model provides a deterministic prediction of repassivation potential in the sense that for any single value of input solution and alloy chemistry, there is a single predicted repassivation potential. In contrast, the measured repassivation potential has a distributed value. As shown in Figs. 2, 4–7, and 8, the distribution of measured repassivation potentials is especially broad near transition region of inhibition. The distributed nature of the repassivation potential arises from several factors: (1) repassivation potential is a function of crevice geometry, especially crevice gap (tightness). Therefore changes in crevice tightness during the test may affect measured values; (2) although crevice repassivation potential is assumed to be independent of applied charge density above a certain value, in reality it is not completely independent of applied charge density. There is a slight dependence on charge density and the threshold charge density at which the dependence of repassivation potential approaches an asymptotic value may depend on the inhibitor concentration; and (3) we ignore any local chemistry effects in modeling repassivation potential. Underlying this assumption is the observation that at repassivation, the chemistry gradient within pits and crevices disappears. But under potentiokinetic conditions, such gradients may influence the

measured repassivation potential values. This will be especially true for transition points for inhibition, where small concentration gradients within a crevice may significantly influence local repassivation.

5. Conclusions

Repassivation potentials have been investigated for selected stainless steels and nickel-base alloys in aqueous environments containing chlorides as aggressive species and various oxyanions as inhibitors. A matrix of repassivation potential data has been established for alloys 316L, 600, 690, 254SMO, 2205, and S-13Cr in the presence of various combinations of chlorides with hydroxides, molybdates, vanadates, sulfates, and nitrates. A previously developed mechanistic model for calculating the repassivation potential has been shown to reproduce the data with very good accuracy. In particular, the model predicts the transition from the concentration range in which localized corrosion is possible to the region in which inhibition is expected. To enhance the predictive character of the model, its parameters have been correlated with alloy composition for Fe–Ni–Cr–Mo–W–N alloys. This correlation makes it possible to predict the repassivation potential for alloys for which experimental data are not available.

Acknowledgements

The work reported here has been supported by the U.S. Department of Energy (award number DE-FC36-04GO14043) and cosponsored by ChevronTexaco, DuPont, Haynes International, Mitsubishi Chemical, Shell, and Toyo Engineering. The contribution to the experimental data by C. Sean Brossia is gratefully acknowledged. Messrs. Brian Derby, John Duck, and Carlos Lopez conducted the experiments reported in this paper.

References

[1] R.W. Staehle, B.F. Brown, J. Kruger, A. Agarwal (Eds.), U.R. Evans Conference on Localized Corrosion, TX NACE International, NACE-3, Houston, 1974.
[2] Z. Szklarska-Smialowska, Pitting Corrosion of Metals, NACE International, Houston, 1986.
[3] H.S. Isaacs, U. Bertocci, J. Kruger, Z. Smialowska (Eds.), Advances in Localized Corrosion, NACE International, NACE-9, Houston, TX, 1990.
[4] P.M. Natishan, R.G. Kelly, G.S. Frankel, R.C. Newman (Eds.), Critical Factors in Localized Corrosion, The Electrochemical Society, Pennington, NJ, 1996, pp. 95-15.
[5] P.M. Natishan, H.S. Isaacs, M. Janik-Czachor, V.A. Macagno, P. Marcus, M. Seo (Eds.), Passivity and Its Breakdown, The Electrochemical Society, Pennington, NJ, 1998. pp. 97-26.
[6] M. Seo, B. Macdougall, H. Takahashi, R.G. Kelly (Eds.), Passivity and Its Breakdown, The Electrochemical Society, Pennington, NJ, 1999. pp. 99-27.
[7] A. Anderko, N. Sridhar, D.S. Dunn, Corros. Sci. 46 (2004) 1583.
[8] N. Sridhar, C.S. Brossia, D.S. Dunn, A. Anderko, Corrosion 60 (2004) 915.
[9] D.S. Dunn, G.A. Cragnolino, N. Sridhar, Corrosion 56 (2000) 90.
[10] D.S. Dunn, N. Sridhar, G.A. Cragnolino, Corrosion 52 (1996) 115.
[11] A. Anderko, N. Sridhar, L.T. Yang, S.L. Grise, B.J. Saldanha, M.H. Dorsey, Corros. Eng. Sci. Tech. 40 (2005) 33.
[12] H.H. Strehblow, B. Titze, Corros. Sci. 17 (1977) 461.
[13] F. Jallerat, L. Pari, F. Bourelier, K. Quang, in: Proceeding of the Nineth International Congress on Metallic Corrosion, National Research Council Ottawa, Canada, 1984.
[14] E. McCafferty, J. Electrochem. Soc. 137 (1990) 3731.
[15] B.A. Kehler, G.O. Ilevbare, J.R. Scully, Corrosion 57 (2001) 1042.
[16] D.S. Dunn, Y.-M. Pan, L. Yang, G.A. Cragnolino, Corrosion 61 (2005) 1078.
[17] D.S. Dunn, O. Pensado, Y.-M. Pan, R.T. Pabalan, L. Yang, X. He, K.T. Chiang, Passive and Localized Corrosion of Alloy 22 – Modeling and Experiments, Report CNWRA 2005-02, Southwest Research Institute, 2005.
[18] S. Yang, D.D. Macdonald, Electrochim. Acta 52 (2007) 1871.
[19] J.F. Zemaitis Jr., ACS Symp. Series 133 (1980) 227–246.
[20] M. Rafal, J.W. Berthold, N.C. Scrivner, S.L. Grise, Models for electrolyte solutions, in: S.I. Sandler (Ed.), Models for Thermodynamic and Phase Equilibria Calculations, M. Dekker, New York, NY, 1995, pp. 601–670.
[21] N. Sridhar, in: H.S. Isaacs, U. Bertocci, J. Kruger, S. Smialowska (Eds.), Advances in Localized Corrosion, NACE International, Houston, TX, 1990, p. 263.
[22] E.L. Hibner, Mater. Perform. 26 (3) (1987) 37.
[23] R.C. Newman, Corros. Sci. 25 (1985) 331;
R.C. Newman, Corros. Sci. 25 (1985) 341.
[24] R.S. Lillard, M.P. Jurinski, J.R. Scully, Corrosion 50 (1994) 251.
[25] J.R. Hayes, J.J. Gray, A.W. Szmodis, C.A. Orme, Corrosion 62 (2006) 491.
[26] M. Urquidi-Macdonald, D.D. Macdonald, J. Electrochem. Soc. 136 (1989) 961.
[27] N.J. Laycock, R.C. Newman, Corros. Sci. 39 (1997) 1771.
[28] R.C. Newman, T. Shahrabi, Corros. Sci. 27 (1987) 827.
[29] P.R. Levey, A. van Bennekom, Corrosion 51 (1995) 911.
[30] R.F.A. Jargelius-Pettersson, Corros. Sci. 41 (1999) 1639.
[31] G.P. Halada, D. Kim, C.R. Clayton, Corrosion 52 (1996) 36.
[32] M.H. Moayed, R.C. Newman, Corros. Sci. 40 (1998) 519.
[33] A. Anderko, N. Sridhar, C.S. Brossia, D.S. Dunn, Paper No. 04061, CORROSION/2004, NACE International, New Orleans, LA, 2004.
[34] N. Sridhar, G.A. Cragnolino, Corrosion 49 (1993) 885.
[35] H. Yashiro, K. Tanno, S. Koshiyama, K. Akashi, Corrosion 52 (1996) 109.
[36] C.S. Brossia, G.A. Cragnolino, Corrosion 56 (2000) 505.
[37] J. Postlethwaite, Electrochim. Acta 12 (1967) 333.
[38] G.A. Cragnolino, in: H.S. Isaacs (Ed.), Advances in localized corrosion, Proceedings of the Second Conference on Localized Corrosion, Orlando, FL, 1987.
[39] K.S. Pitzer, Thermodynamics, third ed., McGraw-Hill, New York, NY, 1995.